Solar Physics (2006) 239: 393–436
DOI: 10.1007/s11207-006-0133-2

PROPERTIES OF INTERPLANETARY CORONAL MASS EJECTIONS AT ONE AU DURING 1995 – 2004

L. JIAN
Institute of Geophysics and Planetary Physics, University of California, Los Angeles, 595 Charles E. Young Dr. East, 6862 Slichter, Los Angeles, CA 90095, U.S.A.
(e-mail: jlan@igpp.ucla.edu)

C.T. RUSSELL
Institute of Geophysics and Planetary Physics, University of California, Los Angeles, 595 Charles E. Young Dr. East, 6869 Slichter, Los Angeles, CA 90095, U.S.A.
(e-mail: ctrussel@igpp.ucla.edu)

J.G. LUHMANN
Space Sciences Laboratory, University of California, Berkeley, CA 94720, U.S.A.
(e-mail: jgluhman@ssl.berkeley.edu)

and

R.M. SKOUG
Los Alamos National Laboratory, Los Alamos, NM 87545, U.S.A.
(e-mail: rskoug@lanl.gov)

(Received 10 January 2006; accepted 11 September 2006; Published online 28 November 2006)

Abstract. We present a comprehensive survey of 230 interplanetary CMEs (ICMEs) during 1995 – 2004 using *Wind* and ACE *in situ* observations near one AU, and examine the solar-cycle variation of the occurrence rate, shock association rate, scale size, velocity change, and other properties of ICMEs. The ICME occurrence rate increases (from 5 in 1996 to 40 in 2001) with solar activity; and 66% of all ICMEs occurred with shock(s). A compound parameter, the total pressure perpendicular to the magnetic field (*Pt*), *i.e.*, the sum of magnetic and perpendicular plasma thermal pressures, assists us in effectively distinguishing ICMEs from other solar-wind structures such as stream interactions, and in quantifying the interaction strength. We interpret the characteristic signatures of the *Pt* temporal variation in terms of the inferred distance perpendicular to the flow to the center of the obstacle. Group 1 includes events that appear to be traversed near the ICME center, showing an apparent enhanced central *Pt*; Group 3 represents ICMEs passed far away from the center, displaying a rapid rise and then gradual decay in *Pt*; and Group 2 includes events with intermediate signatures. About 36% of 198 classifiable ICMEs are Group 1 events, consistent with the conventional wisdom that at one AU a magnetic cloud is found during crossings of only ∼1/3 of ICMEs. Our set of Group 1 ICMEs and the set of magnetic clouds from other researchers have significant overlap and a similar solar-cycle dependence. The rough decline of the Group 1 fraction as solar activity increases, is consistent with rough increases of scale size, shock percentage, and peak *Pt*. These results call into question the need to have different mechanisms to create differently appearing ICMEs. Rather it is possible that all ICMEs have a central flux rope that is traversed about 33% of the time, but in the majority of cases is missed by the spacecraft.

Electronic Supplementary Material Supplementary material is available for this article at *http://dx.doi.org/10.1007/s11207-006-0133-2*

1. Introduction

Coronal mass ejections (CMEs), seen in light scattered from enhanced electron densities in the solar corona (*e.g.* Gosling, Pizzo, and Bame, 1973; Gosling, 1990 and references therein), are transient events with large amounts of material ejected from the solar atmosphere (*e.g.*, Hundhausen, 1988; Kahler, 1988). They play an important role in the long-term evolution of the corona (Hundhausen, 1999). Interplanetary CMEs (ICMEs), *i.e.*, the interplanetary manifestations of CMEs, have been studied since the early decades of solar wind observations, as reviewed by Gosling (1990), Neugebauer and Goldstein (1997), and Rust (1999). Figure 1 is a simplified paradigm of an ICME, showing that the ICME frequently has a leading shock (or shock wave) and a well-formed, perhaps force-free flux rope at the center of the disturbance. In actuality by one AU, when the magnetic stresses are weaker relative to those in the plasma, the flux rope could deviate from the depicted dipolar shape and may not have such a circular cross section any more.

Since near the Earth, the density enhancement that defines a CME back at the Sun is generally not so evident, the identification of ICMEs is usually based on patterns of change in other properties of the magnetized plasma: a stronger than ambient magnetic field, rotating magnetic field (*e.g.*, Hirshberg and Colburn, 1969; Burlaga *et al.*, 1981; Klein and Burlaga, 1982), declining velocity (*e.g.*, Klein and Burlaga, 1982; Russell and Shinde, 2003), low β (ratio of the plasma thermal pressure to the magnetic pressure), abnormally low proton temperature (*e.g.*, Gosling, Pizzo, and Bame, 1973; Richardson and Cane, 1995), low electron temperature (*e.g.*, Montgomery *et al.*, 1974), bidirectional solar wind electron strahls (BDEs) (*e.g.*, Zwickl *et al.*, 1983; Gosling *et al.*, 1987), plasma-compositional anomalies (*e.g.*, Hirshberg, Bame, and Robbins, 1972; Bame

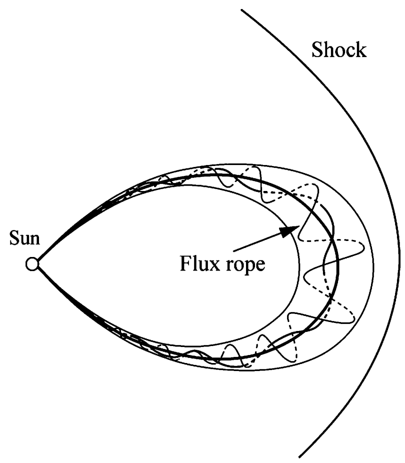

Figure 1. Simplified paradigm of Interplanetary Coronal Mass Ejection (ICME).

et al., 1979; Ipavich *et al.*, 1986; Goldstein, Neugebauer, and Clay, 1998), abnormal charge state of ions (*e.g.*, Lepri *et al.*, 2001), energetic particle signatures (*e.g.*, Morrison, 1956; Palmer, Allum, and Singer, 1978; Marsden *et al.*, 1987; Richardson, Cane, and von Rosenvinge, 1991) and others. None of these features appears to be unique to ICMEs or by itself a sufficient condition to identify an ICME (*e.g.*, Gosling, 1997; Neugebauer and Goldstein, 1997). Furthermore, some of these parameters are not consistently available.

Because the above signatures of ICMEs arise from different physical conditions, such as plasma heating near the Sun during CME formation, expansion in the solar wind, and large-scale field structures, which may be rooted at the Sun, or reconnect with the interplanetary magnetic field (IMF), they may not occur exactly concurrently (*e.g.*, Richardson and Cane, 2005). In fact, any of these characteristics could be missing and, if the others were present, some observers would argue for the presence of an ICME. For instance, some ICMEs or parts of ICMEs lack a BDE signature (*e.g.*, Gosling, Birn, and Hesse, 1995; Shodhan *et al.*, 2000); on the other hand, not only ICMEs, but shocks near the co-rotating interaction regions (CIRs) and magnetic connection of the IMF with planetary bow shocks, can also cause BDEs (*e.g.*, Ogilvie, Scudder, and Sugiura, 1971; Feldman *et al.*, 1973, 1982, 1983; Gosling *et al.*, 1993; Steinberg *et al.*, 2005). Also, some ICMEs lack a helium abundance enhancement (*e.g.*, Zwickl *et al.*, 1983; Phillips *et al.*, 1995). So, based on varied criteria, several research groups have compiled lists of ICMEs, which are somewhat different from each other, *e.g.*, Larson (*http://sprg.ssl.berkeley.edu/~davin/clouds/cloud_list.html*); Lepping (*http://lepmfi.gsfc.nasa.gov/mfi/mag_cloud_pub1.html*); Cane and Richardson (2003); Liu, Richardson, and Belcher (2005); Russell and Shinde (2005).

The magnetic clouds (MCs) form a specific subset of ICMEs, and they are characterized by a low β and by large coherent internal magnetic field rotations through a relatively large angle (Burlaga *et al.*, 1981; Klein and Burlaga, 1982; Lepping, Jones, and Burlaga, 1990; Burlaga, 1991). Gosling (1990) concluded that about 30% of ICMEs at one AU exhibited magnetic flux ropes. However, it is not possible to show that 70% of ICMEs at one AU in fact lack a flux rope, because of the limitation of single-point observations. From the observations at one AU during solar cycles 20 – 21, 23 and also of *Helios* 1 and 2 at 0.3 – 1.0 AU, Richardson and Cane (2004) reported a rough decrease in the MC fraction as the solar activity level increases. Different mechanisms have been proposed to form ICMEs, but because of the dominant role of the magnetic field in the eruption process through the conversion of magnetic energy into kinetic energy, modelers have not yet been able to devise a process that could produce a CME without an embedded flux rope (Riley *et al.*, 2006).

So, it is possible that ICMEs all contain a well-defined flux rope close to the Sun (Marubashi, 1997), but that some flux rope signatures have weakened as the ICME evolves on its way to one AU (*e.g.*, Osherovich and Burlaga, 1997). Alternatively, ICMEs may continue to contain identifiable flux ropes out to one AU, but some of them are traversed far from the central flux rope where the flux rope can not be detected (*e.g.*, Jian *et al.*, 2005a; Riley *et al.*, 2006). We address this proposition in detail below.

It is very appropriate to undertake this comprehensive study of a solar cycle of ICME activity at the present time. First, the *Wind* and *Advanced Composition Explorer* (ACE) spacecraft have just now obtained a sufficiently long data set to enable such a study to be undertaken. Second, we stand at the threshold of a new set of such data from the *Solar-Terrestrial Relations Observatory* (STEREO) mission, for which this study could aid in the interpretation. By determining the solar-cycle dependence of ICMEs we can place the early STEREO data at solar minimum into better context. Third, this study provides a baseline with which to compare data taken at distances closer to and further from the Sun, studies which we plan to undertake in the near future.

2. Total Perpendicular Pressure

Despite some well-developed physical models, some of which include launching CMEs and following them to Earth (*e.g.*, Odstrcil and Pizzo, 1999a,b,c; Linker *et al.*, 2003; Riley *et al.*, 2003; Manchester *et al.*, 2004), there is no thorough understanding of key aspects of CMEs, specifically, how they are initiated in the solar corona, and how they evolve to produce the signatures appearing in the *in situ* observations (Linker *et al.*, 2003). It may be possible to improve our understanding with a new approach to choosing the plasma and field parameters to describe ICMEs, by moving away from specific measurements dictated by instrument outputs to a more physically-based parameter that controls the dynamics of the plasma.

Occasionally such a physically-based parameter, total pressure, has been used to characterize typical ICMEs (*e.g.*, Gosling *et al.*, 1987, 1994; Gosling, 1990), but it has not been utilized in a comprehensive study. Since the magnetic field does not exert a pressure force parallel to the field, the total perpendicular pressure (*Pt*), the sum of the magnetic pressure and plasma thermal pressure perpendicular to the magnetic field [$B^2/(2\mu_0) + \sum_j n_j k T_{\mathrm{perp},j}$, where j represents proton, electron and α particle] is the key pressure component in determining the evolution of these magnetic structures (Russell, Shinde, and Jian, 2005).

If magnetic field lines are straight (no magnetic curvature force), *Pt* should tend to be slowly varying in the absence of the interaction with an obstacle, because unbalanced compressions lead to propagating waves that smooth the pressure profile. If there is a collision of the plasma with an obstacle, a force (gradient in the pressure) will occur that slows and deflects the plasma around the obstacle.

If field lines are not straight, the magnetic curvature force (twist in the rope) can contribute significantly to enhancing the magnetic field strength. It may even be self-balancing such as in a force-free flux rope. Hence, our simple pressure balance calculation (that implicitly assumes straight field lines) is insufficient to describe the force within a flux rope, and will overestimate the pressure. This should be noticeable in the tightly twisted field lines in the cores of ICMEs.

Our many case studies illustrate that much simpler signatures are found in *Pt* than in its constituent components for solar wind structures. The *Pt* is a good diagnostic of solar wind internal dynamics, be it an ICME or a stream interaction region (SIR), driven by fast wind overtaking slow wind (*e.g.*, Gosling and Pizzo, 1999). In conjunction with the features of solar wind velocity, vector magnetic field and other parameters, *Pt* is an effective complementary parameter to distinguish ICMEs and SIRs. Moreover, it can quantify the interaction strength.

3. Our Criteria, Data Set, and List of ICMEs

In our study, the ICMEs are identified by eye from a combination of the *Pt* elevation, and the expected signatures of magnetic field and plasma addressed in Section 1, such as, the low proton temperature, a stronger than ambient magnetic field, a relatively quiet and smooth rotation in magnetic field, a helium abundance enhancement, BDE. However, none of these above characteristics, even the *Pt* enhancement, is a necessary condition when some other features of plasma and magnetic field are prominent. This explains why we have found some ICMEs with peak pressure ($P_{\max}$) lower than 50 pPa. For some ambiguous events, we also check the SOHO Large Angle and Spectrometric Coronagraph (LASCO) (Brueckner *et al.*, 1995) CME catalog (*http://lasco-www.nrl.navy.mil/daily_mpg/; http://cdaw.gsfc.nasa.gov/CME list/*) to assure our identification.

Since it is hard to separate the magnetic obstacle from the magnetosheath region for some ICMEs, to be consistent and comparable, we set the boundary of all ICMEs associated with the outer distinct plasma and magnetic field discontinuities, often indicated by a rapid *Pt* jump. Therefore, our ICMEs include the shock (if it occurs), sheath pile-up region and the ejecta driver. For all the events with apparent magnetic obstacle structures, we give the start time of magnetic obstacle in the third column of the Appendix*, with its end time being the same as the whole event.

We use the *Wind* [SWE (Ogilvie *et al.*, 1995) and MFI (Lepping *et al.*, 1995), both in 93-second time-resolution] solar wind data set and the ACE [validated Level 2 of SWEPAM (McComas *et al.*, 1998) and MAG (Smith *et al.*, 1998), both in 64-second time-resolution] solar wind data set. Because the measurement of electron temperature (T_e), the ratio of number density of α to proton, α temperature, and the anisotropy of particle temperature, are not continuously available, we need to make some assumptions to calculate the *Pt*.

*A tab-delimited text file of the Appendix is available as Electronic Supplementary Material at http://dx.doi.org/10.1007/s11207-006-0133-2 and is accessible for authorised users. It can be imported into MS Excel or other spreadsheet software.

Electrons have high thermal conductivity, so their temperature generally varies in a small range and bears little correlation with other solar wind parameters (Newbury *et al.*, 1998, and references therein). The average electron core temperature near one AU changes only from 123 000 K around solar minimum to 144 000 K near solar maximum (Issautier *et al.*, 2005). Thus, we assume a constant solar wind electron perpendicular temperature of 130 000 K, which is also close to the median value of Newbury *et al.* (1998) from ISEE-3 measurements (August, 1978 – March, 1980). Because the α particles contribute a lesser amount to *Pt*, we assume a constant 4% fraction of α particles by number with a temperature four times proton temperature. Without specific perpendicular temperatures for protons and α particles, we additionally assume that these temperatures are isotropic.

Wind and ACE both are close to the ecliptic plane at about one AU; ACE at the Lagrange L_1 point, while *Wind* was originally positioned in a sunward, multiple double-lunar swingby orbit with a maximum apogee of 250 R_e during its first two operation years, followed by a halo orbit at the Earth–Sun L_1 point, a distant prograde orbit with excursions of 300 R_e in the Y_{GSE} direction, and a trip to L_2, until now placed in a halo orbit about L_1. Hence, the use of the two spacecraft introduces a certain amount of variation in the timing of signatures of about one hour or so. However, ICMEs are large-scale spatial structures, with an average radial width of $\sim$0.25 AU at the Earth's orbit (*e.g.*, Klein and Burlaga, 1982), resulting in similar properties observed at the two spacecraft most of the time.

Because of its longer coverage, we derive our survey of ICMEs mostly from *Wind*. But in order to create as complete a list of ICMEs as possible, when *Wind* is too close to the Earth where the solar wind may be deflected by the Earth's magnetosphere, or it has data gaps or noisy data, we use ACE data, marked as "ACE" in the comments of the Appendix. From 1995 to 1997, *Wind* has data gaps or noise during only 3.8%, 7.6%, and 3.7% of each year, respectively. We did not adjust our statistical results for these small outages as they are smaller than the expected statistical variability.

Using 1995 – 2004 *Wind* and 1998 – 2004 ACE solar wind data, we have identified 230 ICMEs to provide a comprehensive survey of ICMEs in the near-Earth solar wind (see Appendix), encompassing the end of solar activity cycle 22 and the rising, maximum and partially the declining phases of solar cycle 23. The annual average ICME event number is 23, but we do not rule out the possibility that we missed some events due to data gaps, noise and ambiguous ICME signatures. By examining the surrounding solar wind context, we also mark some hybrid events by a star in the Appendix.

The geomagnetic effects depend principally on the IMF (*e.g.*, Russell and McPherron, 1973) and the solar wind velocity. So, we are most interested in these two quantities. Since the *Pt* in ambient solar wind is about 20 – 30 pPa, usually much less than the pressure of ICMEs, and in addition because we are concerned with the comparison between events, rather than an absolute value of pressure of each event, we just consider the magnitude of *Pt* rather than the difference between it and the background pressure. In the survey, we denote ΔP as the instantaneous change of the *Pt* across the discontinuity, $B_{\max}$ as the peak of $|\mathbf{B}|$, R_V as the ratio of $V_{\max}$ to $V_{\min}$, ΔV as the change in the solar wind speed during each event. We emphasize that most ICMEs have a declining solar wind velocity (*e.g.*, Klein and Burlaga, 1982; Russell and Shinde, 2003) with a negative value of ΔV.

For a discontinuity simply indicated by *Pt*, we examine the $\boldsymbol{V}_p$, N_p, T_p, and $\mathbf{B}$ one by one, sometime also use the higher time-resolution Wind 3DP (Lin *et al.*, 1995) and MFI, ACE SWEPAM and magnetometer data from CDAWeb, to verify if these parameters simultaneously vary and whether the discontinuity is a forward or reverse shock. In addition, we have compared our shock identification with the shock lists from Kasper (*http://space.mit.edu/home/jck/shockdb/shockdb.html*) and the ACE MAG and SWEPAM team (*http://www-ssg.sr.unh.edu/mag/ace/ACElists/obs_list.html*) to confirm identifications.

4. Three Groups of ICMEs

It was evident early in the study that the temporal behavior of *Pt* in ICMEs displays characteristic patterns, that can be categorized into three groups (Jian *et al.*, 2005a,b; Russell, Shinde, and Jian, 2005), illustrated by the three examples in Figures 2–4. These three figures have the same format, displaying several of the main parameters we use to characterize ICMEs. In the first three panels, we plot B_x/B, B_y/B, B_z/B, the direction cosines of IMF in the GSM coordinates. We do not use another common pair of angles, cone angle, arccos (B_x/B) and clock angle, arctan (B_y/B_z) of IMF, because these two angles do not order the properties of ICMEs at one AU. Use of GSM coordinates will help in future studies of geoeffectiveness. The following panels are respectively $|\mathbf{B}|$ as the magnetic field magnitude, V_p as the solar wind bulk velocity magnitude, N_p as the proton number density, T_p as the proton temperature, β the ratio of plasma pressure to magnetic pressure, and total perpendicular pressure, *Pt*, in the unit of pico-Pascal (pPa).

Figure 2 presents a typical Group 1 (G1) ICME, the shock and magnetosheath (the region between dashed lines *a* and *b*) are followed by the magnetic obstacle (the region between dashed lines *b* and *c*), *Pt* increases rapidly at the sheath and piles up to a central maximum in the later magnetic obstacle. We can observe such well-defined MCs as shown in Figure 2, in most G1 events, but not all G1 events have obvious shocks. Group 2 (G2) ICMEs have a rapid rise in *Pt*, again, not necessarily a shock (a shock is not a required criterion for ICME identification), with a pressure plateau and a much later return to earlier lower pressure (Figure 3). Among G2 events, we can see some signatures of MCs, but they are less obvious than G1. In Group 3 (G3) ICMEs, the pressure profile usually rises rapidly and then

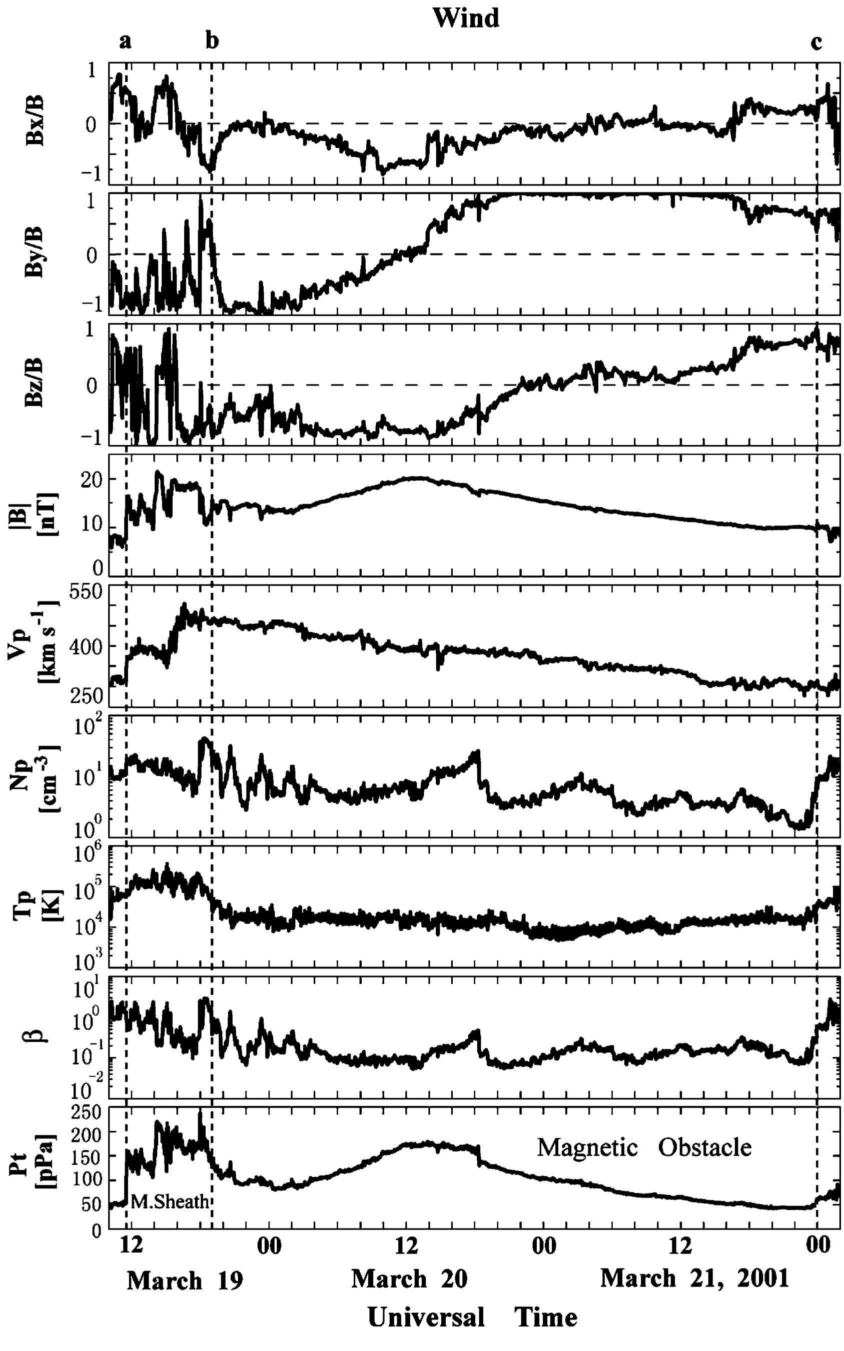

Figure 2. Group 1 ICME from *Wind* observation. From top to bottom: direction cosines of IMF in GSM coordinates, magnetic-field strength, solar-wind speed, proton density, proton temperature, β, and total perpendicular pressure. M. Sheath: magnetosheath, the interval between the dashed lines *a* and *b*; magnetic obstacle, the region between dashed lines *b* and *c*.

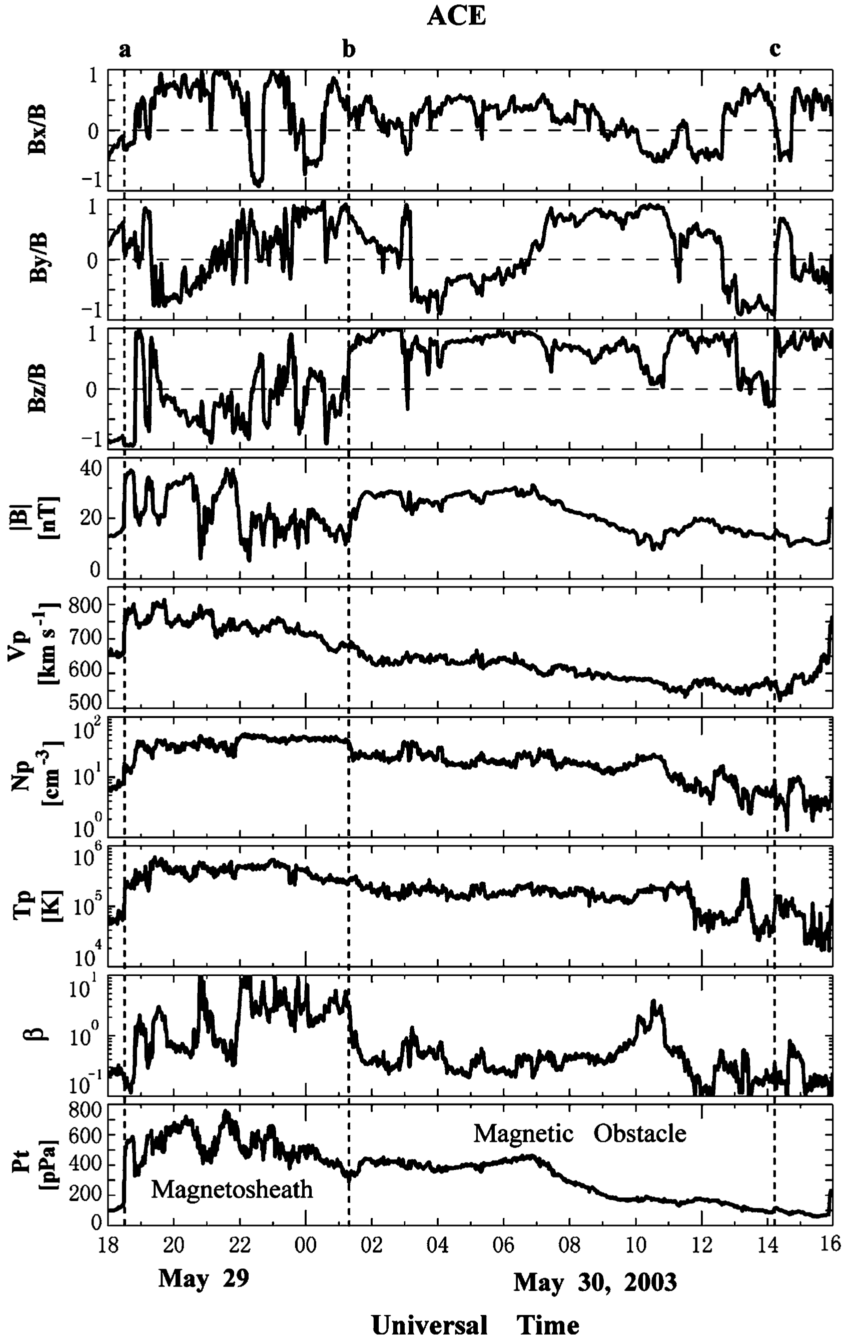

Figure 3. Group 2 ICME from ACE observation. Comments in the caption of Figure 2 apply.

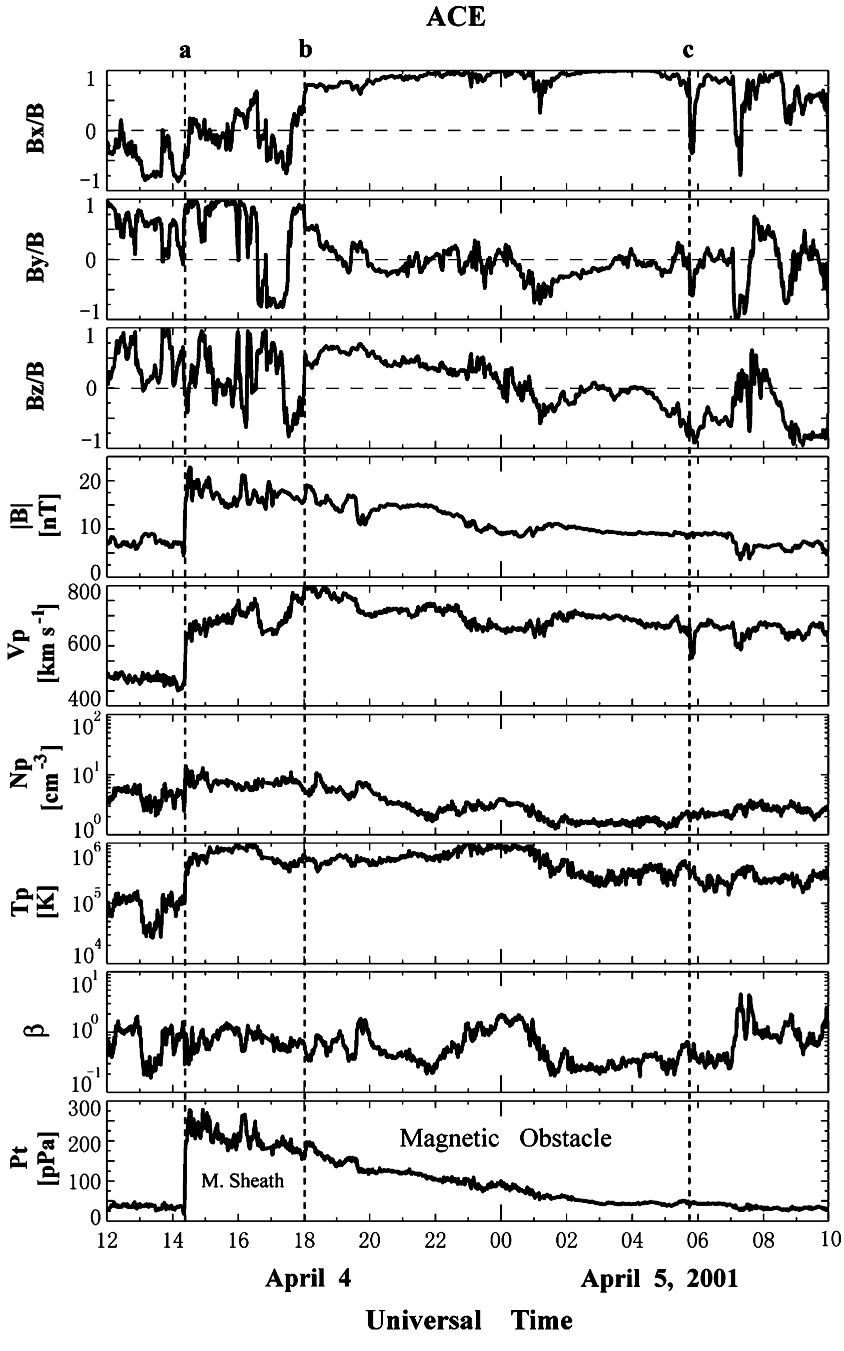

Figure 4. Group 3 ICME from ACE observation. Comments in the caption of Figure 2 apply. As a clear example of Group 3 ICMEs, we can still see the magnetic obstacle from the magnetic field measurements between dashed lines *b* and *c*. But for 92% of the Group 3 events, magnetic obstacles can not be well discerned.

gradually decays over hours or days. During such cases, the individual features of the MC, such as the stronger than ambient and rotating magnetic field, are usually not recognizable. Figure 4 shows a relatively clear G3 example, where we can still see traces of the magnetic obstacle from the magnetic field measurements. However, it is hard to discern the obstacle solely from the plasma observation and compound parameters β and *Pt*.

Hence, the presence of MC signatures is correlated with the *Pt* profiles. Considering the center of magnetic obstacle usually has larger pressure than in other regions, the G1 events appear to mark the passage of the ICME through or near the center of ICMEs, where we see the MC signatures. The G3 event with few MC signatures, appear to be just glancing encounters. Thus, the different patterns of the *Pt* profile may indicate different impact parameters of spacecraft relative to the center of ICMEs. If there is a flux rope in the center of ICME, the dynamic (expanding or just moving faster than the solar wind) ICMEs should create a disturbance in the ambient solar wind greater than the size of the embedded flux rope. Spacecraft that do not penetrate the central region of an ICME will not always see the simple MC structure drawn in Figure 1.

In Figure 5, we have drawn a flux rope in the place of the magnetosphere used as the obstacle to the flow in the Spreiter, Summers, and Alksne (1966) gas-dynamic simulation of flow passing a blunt object. The contours show the density which we take as a rough proxy for the pressure. We are aware that the CME will undergo considerable distortion as it moves away from the Sun and may have complicated geometry by the time it reaches one AU (*e.g.*, Odstrcil and Pizzo, 1999c; Riley *et al.*, 2003), in contrast to the circularly symmetric flux rope as shown in Figure 5. We interpret our three groups of ICMEs as corresponding to different distances of the spacecraft passes through the ICME relative to the central flux rope (origin in Figure 5). These trajectories are marked in Figure 5 by arrows.

Nevertheless, the above sorting is idealized and the variation from Group 1 to 3 is a continuum with somewhat arbitrary definitions. For example, over the ten years of our study, 8% of the G3 ICMEs appear to traverse a part of a magnetic obstacle. The spacecraft may only pass a part of cloud, without seeing a complete cloud structure. We emphasize that the patterns form a continuum without sharp boundaries between the categories.

In contrast to the ICME *Pt* profiles, the SIRs usually have a peak with a slow increase and decrease of pressure on its two sides (*e.g.*, Gosling and Pizzo, 1999; Jian *et al.*, 2006), indicating the forces pushing outward to the two sides of the stream interface. However, many CMEs observed at the Sun are slow (*e.g.*, Gosling *et al.*, 1976), and they may be difficult to distinguish from SIRs just by their pressure profile, unless they have sufficient internal pressure and expansion to produce a shock. But from the plasma and magnetic field features, composition signatures (*e.g.*, α particles abundance) and electron topology (BDEs), it is also possible to distinguish them.

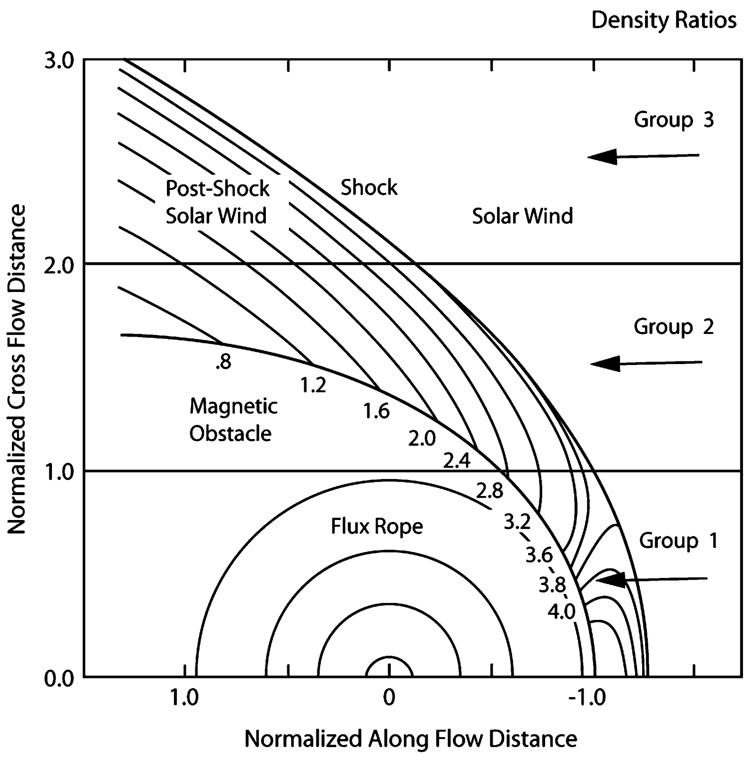

Figure 5. Interpretive sketch of ICME encounters using Spreiter, Summers, and Alksne (1966) gas-dynamic simulation results. Group 1 events encounter the magnetic rope. Group 2 events encounter the ICME near the obstacle. Group 3 events catch the shock away from the obstacle. In reality, the magnetic rope is not circularly symmetric but distorted.

5. Occurrence Rate of ICMEs

The annual number of ICMEs from 1995 to 2004 is given in Table I, and also shown in panel (a) of Figure 6. The ICME occurrence rate varies greatly, from 5 in 1996, around solar minimum, up to 40 in 2001, near solar maximum (consistent with the largest halo CME number in 2001, halo CME number from SOHO LASCO CME catalog), increasing monotonically except for 1999 as the solar activity level increases. The unusually low occurrence rate in 1999 is also noted in Cane, Richardson, and St. Cyr (2000) and Cane and Richardson (2003), probably associated with an increase of co-rotating high-speed streams from low-latitude coronal holes and the restructuring of the near-ecliptic solar wind in 1999 (*e.g.*, Luhmann *et al.*, 2002; Cane and Richardson, 2003).

We classify 198 ICMEs with clear *Pt* characteristics into three groups. Table I shows the number in each group of ICMEs as well as their relative occurrence rate.

TABLE I

Comparison of ICMEs in the three groups and with other lists.

	ICME												
	Group 1		Group 2		Group 3		Total ICME No.		$C + R$[a]	Overlap of our list	$C + R$	Lepping[c]
Year	No.	%	No.	%	No.	%	in the 3 Groups	ICME No.	ICMEs No.	and $C + R$ list	MC[b]s No.	MCs No.
1995	5	50.00	4	40.00	1	10.00	10	11	NA	NA	NA	8
1996	4	80.00	1	20.00	0	0.00	5	5	4	4	4	4
1997	11	61.11	5	27.78	2	11.11	18	20	22	18	14	17
1998	8	38.10	8	38.10	5	23.81	21	25	37	22	10	11
1999	6	35.29	5	29.41	6	35.29	17	22	33	18	3	4
2000	14	40.00	4	11.43	17	48.57	35	37	55	33	10	14
2001	7	23.33	6	20.00	17	56.67	30	40	48	28	8	10
2002	7	25.00	5	17.86	16	57.14	28	28	26	20	10	10
2003	5	29.41	6	35.29	6	35.29	17	22	22	19	5	4
2004	4	23.53	5	29.41	8	47.06	17	20	20	17	6	NA
All	71	35.86	49	24.75	78	39.39	198	230	267	179	70	82

[a]$C + R$: List of Cane and Richardson (2003) and private communication in 2006; 1995 event list is not available.
[b]MC: Magnetic cloud.
[c]Lepping: Magnetic cloud list of Lepping (*http://lepmfi.gsfc.nasa.gov/mfi/mag_cloud_pub1.html*).

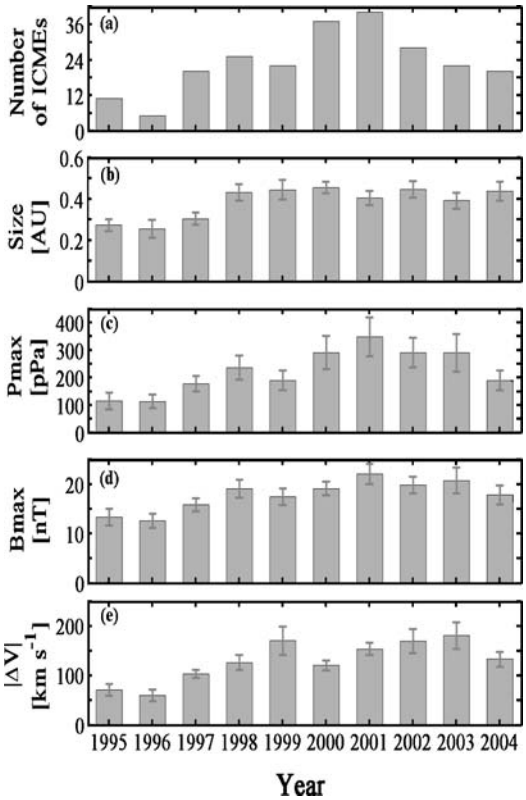

Figure 6. Annual statistics of some properties of ICMEs during the period 1995 – 2004. (a) Occurrence rates of ICMEs. (b) Scale size for each ICME. (c) Peak total perpendicular pressure. (d) Maximum magnetic field. (e) Absolute change in solar wind velocity during one event. The probable error of the mean is indicated.

Among them, there are 71 G1 events, suggesting that on average ∼36% of ICMEs are penerated by *Wind* or ACE near the center of the flux rope. This is consistent with the conventional wisdom that about 1/3 of ICME observations are encounters with MCs at one AU.

Figure 7 illustrates the trend of the percentages of the three groups ICMEs of all the classifiable ICMEs over 1995 – 2004. The extent of the vertical axis is the sum of the three fractions, which is 100% for each year. The occurrence rate of G1 ICMEs (dark gray) [see the left-hand scale], roughly decreases as solar activity strengthens, with a peak at solar minimum; while the occurrence rate of G3 ICMEs (light gray), [see the right-hand scale], has the opposite trend, overtaking the G1 occurrence rate in 2000 – 2002. This anti-correlation of G1 and G3 during the solar cycle is consistent with a stronger dynamic interaction of the ICME with the ambient solar wind around solar maximum (*e.g.*, Riley *et al.*, 2006) causing a larger region of disturbance around the central flux rope. This

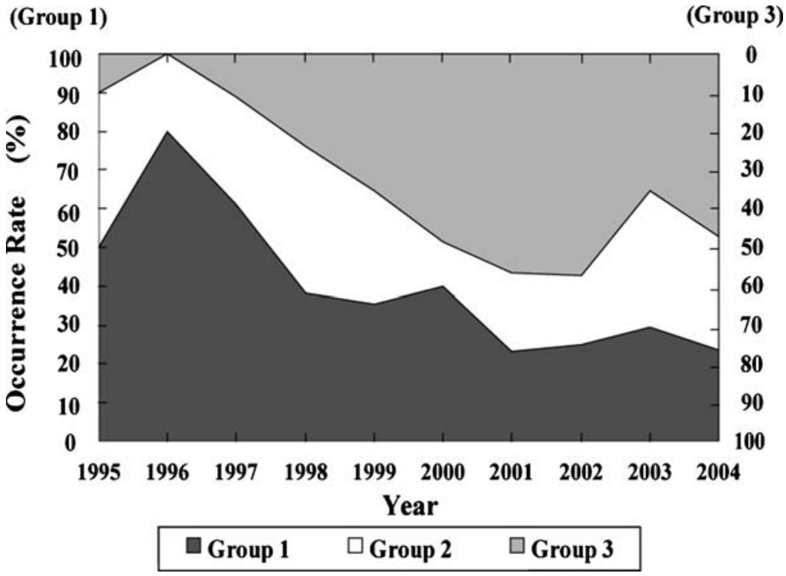

Figure 7. Occurrence rates of ICMEs in three groups during 1995 – 2004.

hypothesis is consistent with the rough increases of P_{max}, scale size, and shock associations. The white region between the two gray areas represents the percentage of G2 ICMEs, without much variation over the 10 years, being smallest in 2000.

In addition, there are 32 events too complicated to be sorted into any of the three groups. Some of them are hybrid events of ICME and SIR or of more than one ICME, and others have some irregular pressure profiles, often with extremely low Pt. We note that if they could be classified as members of one of the three groups, the statistics would change but slightly.

In Table I, we also list the number of our identified ICMEs and compare them with ICMEs identified by Cane and Richardson (2003, and private communication in 2006) (hereinafter referred to as CR). They did not classify ICMEs in the available 1995 data. The CR study used quite a few characteristics such as low proton temperature, reduced magnetic field fluctuations, and other criteria. We also list MCs identified by Lepping for each year from 1995 to 2003. The ICME rates given from the three research groups have similar solar-cycle dependence. But for the period 1998 – 2000, CR find over ten events per year more than we do, possibly because they have also used *Interplanetary Monitoring Platform* (IMP 8) data and additional criteria. As they intended, this study should have produced the most liberal or inclusive list. We note that taking many signatures (*e.g.*, solar energetic particles, cosmic ray, *etc.*) into account, will reduce the influence of the plasma and field parameters on the identifications.

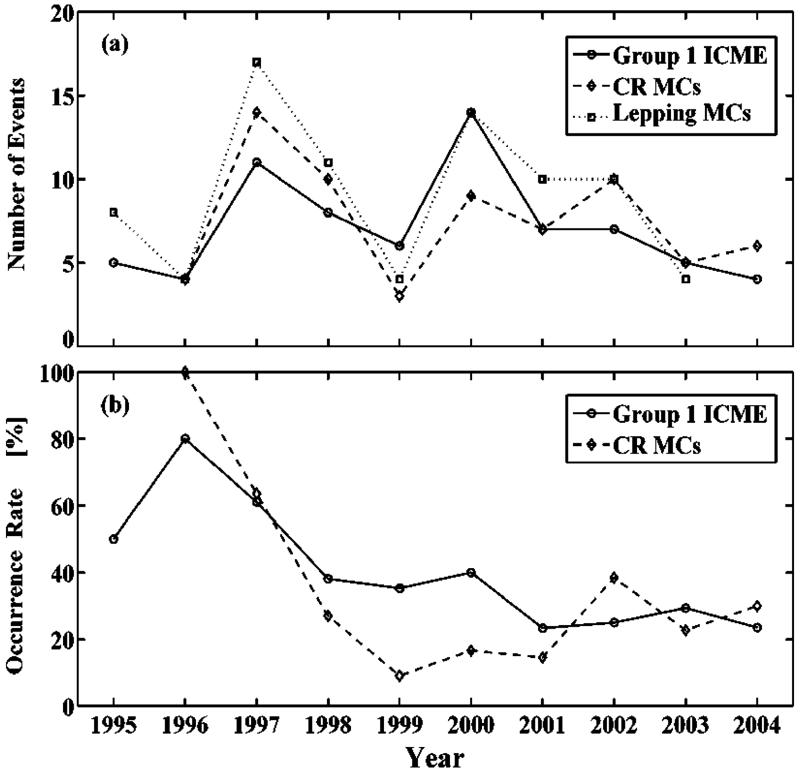

Figure 8. (a) Comparison of the number of events of our identified Group 1 ICME and magnetic clouds (MCs) identified by Cane and Richardson and by Lepping. (b) Occurrence rates of Group 1 ICMEs and MCs identified by Cane and Richardson.

We also give the yearly number of overlap events of our study and the CR list in the third-to-last column of Table I. In all from 1996 – 2004, 179 events, accounting for about 82% of our ICMEs are in the CR list, while approximately 67% of their events are in our list. These two statistics indicate that the techniques are different, rather than simply that one is more liberal than the other.

There is an MC quality index in the CR list (0, 1, and 2 indicating increasing quality of the MC). Approximately, 63% of our G1 ICMEs are also in their MC = 2 list, and 26% of our G1 events are in MC = 1 list. Conversely, 18 (accounting for 28%) of their MC = 2 events end up in our G2, and 7 MCs (11%) are in G3. In addition, about 41 events (62%) of our G1 ICMEs were in Lepping's MC table, and on the other hand, 17 cases (39%) of Lepping's MC list end up in our G2, and 8 MCs (11%) are in G3. Considering that our grouping and CR's MC index are both continua with somewhat subjective definitions, the overlap of our G1 ICMEs and other groups' MCs is significant, and the low number of MC signatures in our G2 and G3 lists indicates that these independent approaches are finding consistent results.

Figure 8(a) compares the solar-cycle variations of the number of G1 ICMEs (solid line marked by circles), MCs identified by CR (dashed line marked by diamonds), MCs identified by Lepping (dotted line marked by squares). We can see they have similar solar-cycle dependence. Figure 8(b) shows the percentages of G1 ICMEs relative to all the ICMEs in our study (solid line marked by circles) and MCs relative to all the ICMEs identified by CR (dashed line marked by diamonds). The former is small in 2001 – 2004, while the latter reaches minimum around solar maximum (Richardson and Cane, 2004). The two trends are similar, except for two places on the curve. There is no CR value for our first year 1995. If we use their identified number of ICMEs and MCs for 2004 as indicative of what they would have found in 1995, the curves would be very similar through solar minimum. But we are aware that there is a major difference between 1999 and 2000, where CR identified 30% more ICMEs than we did, but fewer MCs than we did. This again suggests a difference in our criteria for ICME identifications or G1-MC association may not be completely accurate. Nevertheless, their overall result that the portion of magnetic clouds drops at solar maximum, is confirmed by our analysis.

6. Solar-Cycle Variation of Properties of ICMEs

Table II lists the average characteristics of ICMEs observed from 1995 – 2004. It gives the annual number of ICME events, the number and percentage of events

TABLE II

ICME statistics.

Year	ICME No.	% with shock	% with shock	$\langle P_{max} \rangle$ (δP_{max})[a]	$\langle B_{max} \rangle$ (δB_{max})	$\langle R_V = V_{max}/V_{min} \rangle$ (δR_V)	$\langle \lvert \Delta V \rvert \rangle$ $(\delta \lvert \Delta V \rvert)$
1995	11	5	45.5	114.09 (30.40)	13.34 (1.65)	1.22 (0.04)	71.36 (11.37)
1996	5	0	0.0	113.00 (24.27)	12.58 (1.42)	1.18 (0.04)	60.20 (12.16)
1997	20	8	40.0	176.90 (27.67)	15.79 (1.35)	1.31 (0.03)	102.90 (7.90)
1998	25	17	68.0	235.00 (42.51)	18.98 (1.81)	1.34 (0.03)	126.12 (14.50)
1999	22	15	68.2	189.18 (34.89)	17.38 (1.70)	1.44 (0.08)	169.64 (28.73)
2000	37	28	75.7	289.43 (59.69)	19.06 (1.41)	1.29 (0.02)	120.57 (9.81)
2001	40	31	77.5	346.66 (70.75)	21.94 (2.07)	1.36 (0.03)	153.37 (12.87)
2002	28	23	82.1	288.68 (53.54)	19.71 (1.65)	1.44 (0.06)	169.50 (24.13)
2003	22	13	59.1	288.05 (67.52)	20.64 (2.57)	1.37 (0.05)	179.76 (26.33)
2004	20	11	55.0	188.90 (35.96)	17.75 (1.90)	1.33 (0.03)	132.65 (14.93)
All	230	151	65.7	251.59 (19.39)	19.27 (0.71)	1.35 (0.01)	138.89 (6.18)
Max	40	31	82.1	2100	80	2.96	615
Min	5	0	0.0	24	3.5	1.07	30

[a] δ Presents the probable error of the mean for the corresponding parameter.

with shocks, the average $P_{\max}$, $B_{\max}$, R_V, absolute difference of V_p magnitude ($|\Delta V|$) as well as their probable errors of the mean during 1995 – 2004. The bottom three rows list the average, maximum and minimum of these properties among all events. Averaged over the ten years, $P_{\max}$ is 252 ± 19 pPa; $B_{\max}$ is 19.3 ± 0.7 nT; R_V is 1.35 ± 0.01; and $|\Delta V|$ is 139 ± 6 km s^{-1}, where the uncertainty is the probable error of the mean. The R_V and $|\Delta V|$ are smaller than the corresponding values of SIRs, 1.66 ± 0.02, 230 ± 5 km s^{-1} (Jian *et al.*, 2006).

In all, 65.7% of ICMEs drive shocks at one AU. Ten of the ICMEs at one AU began with two or more forward shocks, of which we count as only one forward shock herein. Besides some hybrid events, the other ICMEs are isolated events, but they indeed occur with more than one shock, and these shocks are usually nearly in contact. The fraction of shocks varies roughly in phase with solar activity at one AU, peaking at 82% in 2002. The shock association rate of ICMEs at one AU is much higher than the rate from *Pioneer Venus Orbiter* (PVO) observations (1979 – 1988) at 0.72 AU, where even the highest annual rates are still less than 30% and these occur in the declining phase (Lindsay *et al.*, 1994). While these measurements were made in different solar cycles, they suggest that most ICMEs shocks arise from 0.72 to 1.0 AU. We will address this issue in a future study.

We have found only one single reverse shock, and it is associated with a hybrid event. In all, only three events occurred with forward–reverse shock pairs, and they happened in 2000 – 2001, around solar maximum, with the forward shocks much stronger than the corresponding reverse ones. None of them is associated with overexpansion, verifying that shock pairs associated with overexpansion (Gosling *et al.*, 1994) have never been observed at low heliographic latitudes at any heliocentric distance (Gosling *et al.*, 1995).

The five panels in Figure 6 respectively display the solar-cycle variations of the occurrence rate, scale size, $P_{\max}$, $B_{\max}$ and $|\Delta V|$ of ICMEs from 1995 to 2004, where the error bar is the corresponding probable error of the mean. The ICME annual average duration has no clear solar-cycle dependence, varying from 5.5 to 94 hours, with an average of 35 ± 1 hours.

We use the mean of $V_{\max}$ and $V_{\min}$ as the average velocity, and estimate the scale size of each ICME by the product of average velocity and duration. The size varies from 0.08 to 1.08 AU, and has an average of 0.41 ± 0.01 AU. The annual average size is larger around the solar maximum, except for 2001, again suggesting the ICMEs may affect a larger region during high solar activity. The shock-to-magnetic obstacle sheath region was found on average to be 0.16 AU, with a most probable thickness of 0.13 AU, in an earlier study by Gosling *et al.* (1987). Our result is larger than the size (0.25 AU) found by Klein and Burlaga (1982) two decades ago. This difference is probably due to our inclusion of the pile-up/magnetosheath region in our size estimate.

The value of $P_{\max}$, *i.e.*, the interaction of ICMEs with ambient solar wind or within the ICMEs, increases roughly with the solar activity level, except for 1999.

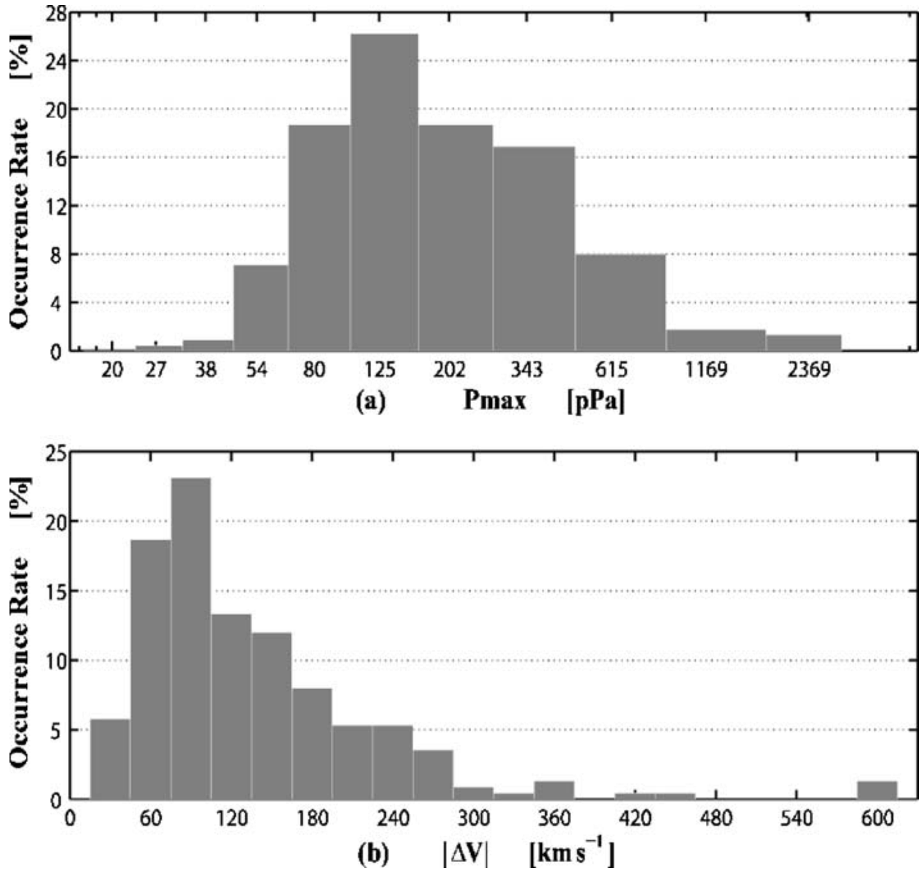

Figure 9. Probability distribution: $P_{\max}$ and $|\Delta V|$ of ICMEs (1995 – 2004).

It varies greatly over the ten years, from the minimum (113 ± 24 pPa) in 1996 to the maximum (347 ± 71 pPa) in 2001. The maximum value is up to three times larger than the minimum. During 2000 – 2003, the variability is over 50 pPa, associated with the large variability of $P_{\max}$ near solar maximum. The value of $B_{\max}$ has a similar solar-cycle variation, with the maximum about twice as large of the minimum. The similarity is expected, because ICMEs are low-β structures and the magnetic pressure makes the largest contribution to Pt.

The annual averages of R_V and $|\Delta V|$ also change much through the ten years. They both reach a minimum around solar minimum and have some large values around solar maximum. Unexpectedly, the two largest R_V values occur in 1999 and 2002, and so does $|\Delta V|$.

The two panels (*a* and *b*) in Figure 9 individually show the probability distributions of $P_{\max}$ and $|\Delta V|$ of these relatively dynamically active ICMEs, one on a quasi-logarithmic scale (to distribute the data well across the bins, we use bin values successively raised by the power 1.1), and the other distribution on a linear scale. They are both almost centrally distributed. The value of P_{max} varies extensively from 24 to 2100 pPa, and is distributed mostly around 125 pPa, where about 26% of ICMEs fall. The $|\Delta V|$ varies from 30 to 615 km s^{-1}, and ∼41% of the 230 ICMEs have the $|\Delta V|$ falling between 45 and 105 km s^{-1}. Moreover, the probability distribution of $|\Delta V|$ has a long tail, caused by some ICMEs with quite large velocity variation.

7. Conclusions

Total perpendicular pressure (*Pt*) in the interplanetary medium near one AU has a simple temporal variation, smooth except for shocks, quiet in contrast to the variations of its individual components. This feature has assisted us greatly in identifying ICMEs.

From 1995 – 2004 *Wind* and ACE solar wind data, we identify 230 ICMEs, and 66% of them occur with shocks, three associated with forward–reverse shocks pairs. The occurrence rates, scale size, P_{max}, B_{max}, and $|\Delta V|$ of ICMEs follow the solar-activity variation, while the duration has no clear solar-cycle dependence. The P_{max} and $|\Delta V|$ both have a broad probability distribution, with the mean values of 252 ± 19 pPa and of 139 ± 6 km s^{-1} respectively. The average size of our ICMEs is 0.41 ± 0.01 AU, and the maximum annual average is about twice the minimum.

Our comprehensive survey of one AU observation of ICMEs can provide a baseline to compare data taken at other heliocentric distances, to further understand the ICME evolution in the heliosphere. It will also help interpret the coming STEREO data, especially in putting STEREO's solar minimum observations in the context of the overall expected solar-cycle variation.

The ICME *Pt* temporal profiles have three characteristic patterns, which are correlated with the observed MC signatures. Corresponding to Group 1, 2, and 3 ICMEs, the *Pt* profile following the shock and/or sheath increases has a central pressure maximum, or a steady plateau, or a gradual decay, respectively. We interpret the three groups of *Pt* profiles as being associated with different distances of approach to the causative central flux rope in each ICME. The absence of an observed flux rope or cloud in the majority of ICMEs does not imply the absence of such a flux rope in the center of the structure.

This interpretation is supported from three aspects in this study. (1) Averaged over ten years, ∼36% of 198 classifiable ICMEs are G1 events, consistent with the general wisdom that about 1/3 of ICME observations at one AU are encounters with magnetic clouds. (2) Our G1 ICMEs and MCs identified by other investigators, mostly overlap and have similar solar-cycle dependence, suggesting that MCs are mainly the G1 ICMEs, which spacecraft pass through the center and observe the expected MC signatures. (3) The fractions of G1 and G3 ICMEs are anti-correlated, and the percentage of G1 (flux rope encountered) roughly decreases as the solar activity enhances, comfirmed by earlier work of Richardson and Cane (2004).

The last variation can have contributions from several factors. The interaction of the flux rope with the ambient solar wind or other ICMEs clearly gets stronger as solar activity strengthens, consistent with rough solar-cycle trends of shock association rate, scale size and P_{max} we have found. Thus, the size of the disturbed region relative to the size of the disturbing central obstacle will change with the solar cycle. Around solar maximum, the latitudinal spread of CME central axes is bigger (Hundhausen, 1993), and a larger fraction of CMEs originate from the mid- or high-heliolatitude of the Sun (*e.g.*, Riley *et al.*, 2006), resulting in a smaller probability of spacecraft in the ecliptic plane passing through the center of ICMEs.

The launch of STEREO will enable multi-spacecraft observations that will allow us to make two or more (using ACE or *Wind*) cuts through ICMEs at varying distances from the center, enabling us to establish the ecliptic longitude variation of these structures and to test our hypothesis that all ICMEs may have central flux ropes, and that the ICME *Pt* signature depends on the impact parameter.

Acknowledgements

This work is supported by the IGPP branch at Los Alamos National Lab (LANL). We have used the *Wind* plasma and magnetic field data throughout. We thank the MIT and Goddard plasma team (A.J. Lazarus and K.W. Ogilvie), 3DP plasma team (R.P. Lin) and the magnetometer team (R.P. Lepping) for making these data available. We have incorporated ACE data in this study with. So we are grateful to the PIs of the plasma analyzer (D.J. McComas) and of the magnetometer (C.W. Smith) for making these data publicly available, and also thank J. Steinberg for collaboration in LANL. Work at Los Alamos was performed under the auspices of the U.S. Department of Energy, with financial support from the NASA ACE program. Moreover, to identify the shocks, we used the higher-time-resolution data in CDAWeb; we thank CDAWeb for making the data available.

APPENDIX

List of Interplanetary Coronal Mass Ejections (ICMEs) from *Wind* and ACE Data over 1995 – 2004. A tab-delimited text file of the Appendix is available as Electronic Supplementary Material at http://dx.doi.org/10.1007/s11207-006-0133-2 and is accessible for authorised users. It can be imported into MS Excel or other spreadsheet software.

#	Start UT (mm/dd hhmm)	Start UT of magnetic obstacle[a] (mm/dd hhmm)	End UT (mm/dd hhmm)	Discontinuity UT	F/R[c] Shock	ΔP[d] (pPa)		P_{max} (pPa)	V_{max} (km s^{-1})	V_{min} (km s^{-1})	ΔV[e] (km s^{-1})	B_{max} (nT)	Group[f]	$C+R$[g]	Lepping[h]	Comments
							1995									
1[b]	02/08 0310	02/08 0310	02/09 0200					88	444	376	−68	12.8	1	/	2	clear **B** rotations
2[b]	02/09 0200		02/10 1000					65	420	340	−80	10.5	3	/	N[i]	
3	03/04 0037	03/04 1142	03/05 0000	03/04 0037	F	23 → 50	27	95 (110)[j]	470	428	−58	13.2	2	/	3	V_p, *Pt* irregular, T_p low, after SIR
				03/04 2000	/	55 → 95	40									
4[b]	03/23 0938	03/24 0000	03/25 2100	03/23 0938	F	30 → 63	33	85 (100)	340 (347)	295	−45	12	2	/	N	followed by an SIR
5[b]	04/03 0100	04/03 0100	04/04 1230					58	356	260	−96	11	2	/	2	*Pt*, B weak
6	05/13 1024		05/14 0515	05/13 1024	/	150 → 90	−60	120	355	315	40	14.6		/	3	complex, *Pt* irregular, like in an SIR
7	06/30 1850	06/30 1850	07/02 1013					80	500	343	−157	11.3	1	/	N	V_{th} ~25 km/s, weak, related to flux rope
8	08/22 1257	08/22 1927	08/23 2100	08/22 1257	F	11 → 35	24	82	383	333	−50	11.8	1	/	2	weak, *Pt* plateau, followed by an SIR
9[b]	10/18 1900	10/18 1900	10/20 0137	10/19 1751	F	200 → 360	160	410	437	378	−59	29	1	/	1	V_p irregular and noisy, in an SIR, shock in the center
10	10/24 0745	10/24 0745	10/25 0804					42	453	340	−113	8	1	/	N	weak, T_p not so low, but B clear rotations

(*Continued on next page*)

APPENDIX
(*Continued*)

#	Start UT (mm/dd hhmm)	Start UT of magnetic obstacle[a] (mm/dd hhmm)	End UT (mm/dd hhmm)	Discontinuity UT	F/R[c] Shock	ΔP[d] (pPa)		P_{max} (pPa)	V_{max} (km s^{-1})	V_{min} (km s^{-1})	ΔV[e] (km s^{-1})	B_{max} (nT)	Group[f]	$C+R$[g]	Lepping[h]	Comments
11[b]	12/16 0450	12/16 0450	12/16 1900	12/15 0437	F	38 → 88	50	100	420	385	−35	12.5	2	/	3	B maximizes during five days, in an SIR
				12/15 1457	/	110 → 80	−30									
				12/16 0450	/	93 → 68	−25									
						1996										
1[b]	02/15 1500	02/15 1500	02/16 0900					105	425	353	−72	10.8	1	N	N	followed by an SIR
2[b]	05/27 1434	05/27 1434	05/29 1120					200	415	340	−75	16.5	1	2	2	following an SIR
3[b]	07/01 1220	07/01 1220	07/02 1435	07/01 1220	/	20 → 40	20	110	370	340	−30	14	1	2	2	irregular *Pt*, following an SIR
				07/01 1417	/	63 → 85	22									
4	08/07 0600	08/07 1100	08/08 0500					50	368	335	−33	8.2	2	2	1	weak, slow ICME
5	12/24 0300	12/24 0300	12/25 1130	12/24 1629	/	97 → 80	−17	100	400	309	−91	13.4	1	2	1	*Wind* impacted the Earth bow shock several times; T_p irregular
						1997										
1[b]	01/10 0050	01/10 0430	01/11 0300	01/10 0050	F	15 → 65	50	380	480	410	−70	20.5	1	2	1	$N_p > 100$ cm^{-3}, T_e extremely low, actual pressure may not be well estimated by *Pt*, followed by SIR
2	02/09 1340	02/10 0245	02/10 1900	02/09 1340	/	30 → 73	43	35 (85)	570 (660)	403	−167	9	1	2	3	
3	02/11 0415	02/11 0415	02/12 0544					103	452	360	−92	7.2	1	N	N	
4[b]	04/11 0552	04/11 0552	04/11 1752					235	490	420	−70	22.8	1	0	2	V_p irregular

(*Continued on next page*)

APPENDIX
(*Continued*)

#	Start UT (mm/dd hhmm)	Start UT of magnetic obstacle[a] (mm/dd hhmm)	End UT (mm/dd hhmm)	Discontinuity UT	F/R[c] Shock	ΔP[d] (pPa)		P_{max} (pPa)	V_{max} (km s^{-1})	V_{min} (km s^{-1})	ΔV[e] (km s^{-1})	B_{max} (nT)	Group[f]	$C+R$[g]	Lepping[h]	Comments
5	04/21 1200	04/21 1200	04/23 0400					120	430	320	−110	14.5	2	2	3	T_p is not low, weak rotations of **B**, *Pt* plateau
6[b]	05/15 0120		05/15 2325	05/15 0120	F	70 → 270	200	280 (360)	500	420	80	26	3	2	2	V_p increases, in an SIR
7	06/07 2330	06/07 2330	06/10 2300					115	415	347	−68	14.3	1	2	2	V_p irregular, only a short interval of low T_p
8	06/19 0012	06/19 0530	06/21 0400	06/19 0012	F	18 → 27	9	52	377 (395)	283	−94	9	2	2	3	plateau, and B_{max} for two days, weak **B** rotations
9	07/15 0905	07/15 0905	07/16 1105					100	380	330	−50	13	2	2	3	noisy
10	08/03 1350	08/03 1350	08/04 0200	08/03 1350	/	130 → 95	−45	140	500	400	−100	17		2	3	a concave in *Pt*
11[b]	09/03 1320	09/03 1320	09/03 2230					175	530	380	150	18	1	0	N	in an SIR, *Wind* passed by the side of ICME
12	09/18 0400	09/18 0400	09/20 1200	09/18 0031	F	45 → 75	30	110	420	270	−150	13.5	1	N	3	T_p not low, V_p decreases and then increases
13[b]	09/21 2205	09/21 2205	09/22 1727	09/21 2205	/	150 → 110	−40	183	490	355	−135	18.5	1	2	2	in an SIR, T_p and V_p increases following the declines
14	10/01 1710	10/01 1710	10/02 2310					65	487	407	−80	10.6	2	2	2	weak, *Pt* plateau, B_{max} for over one day, noisy data before it

(*Continued on next page*)

APPENDIX
(*Continued*)

#	Start UT (mm/dd hhmm)	Start UT of magnetic obstacle[a] (mm/dd hhmm)	End UT (mm/dd hhmm)	Discontinuity UT	F/R[c] Shock	ΔP[d] (pPa)		P_{max} (pPa)	V_{max} (km s^{-1})	V_{min} (km s^{-1})	ΔV[e] (km s^{-1})	B_{max} (nT)	Group[f]	$C + R$[g]	Lepping[h]	Comments
15	10/11 0000	10/11 0000	10/12 0230					95	435	345	−90	13.5	1	2	1	T_p is not low, data gap before it
16	10/27 0620	10/27 0620	10/28 0720					50	555	408	−147	8.8	1	1	N	weak, 2 h data gap, after a big SIR
17	11/06 2220	11/07 0630	11/08 1430	11/06 2220	F	40 → 240	200	150 (270)	470 (480)	330	−140	18.5	1	2	2, 2, but from ACE list only one ICME	plasma data gap at around 11/06 2220, but strong FF[k] from the recovered data[l]
18	11/22 0910	11/22 1850	11/23 1250	11/22 0910	F	45 → 365	320	340 (520)	530	480	−50	26 (31)	2	2	3	
19	12/10 0430		12/12 0000	12/10 0430	F	50 → 200	150	225	430	310	−120	16	3	0	N	ICME meets solar wind and probably magnetic reconnects
20	12/30 0114	12/30 0947	12/31 0647	12/30 0114	F	33 → 93	60	110 (155)	410	315	95	14		1	N	V_p too irregular, two streams with different plasma properties
							1998									
1	01/06 1330	01/07 0250	01/08 0728	01/06 1330	F	60 → 215	155	170 (190)	435	350	−85	19	1	2	1	followed by an SIR
2	01/28 1557	01/29 2010	01/30 2310	01/28 1557	F	30 → 54	24	80	400 (415)	347	−53	9.3	2	0	N	followed by another ICME
3	02/04 0435	02/04 0435	02/05 2200					115	360	290	−70	14.5	1	2	2	
4[b]	02/17 0900	02/17 0900	02/20 0036	02/18 0749	F	150 → 215	65	280	470	360	110	22	1	1, 1[m]	N	T_p enhances at the interface, heated by reconnection? irregular V_p, big deflection of V_p, shock at the center

(*Continued on next page*)

APPENDIX
(*Continued*)

#	Start UT (mm/dd hhmm)	Start UT of magnetic obstacle[a] (mm/dd hhmm)	End UT (mm/dd hhmm)	Discontinuity UT	F/R[c] Shock	ΔP[d] (pPa)		P_{max} (pPa)	V_{max} (km s^{-1})	V_{min} (km s^{-1})	ΔV[e] (km s^{-1})	B_{max} (nT)	Group[f]	$C+R$[g]	Lepping[h]	Comments
5[b]	03/04 1437	03/04 1437	03/06 0200	03/04 1103	F	16 → 36	20	120	395	310	−85	13	1	2	1	
6[b]	03/06 1100	03/06 1100	03/07 2120					65	340	300	−40	8		N	N	
7	05/01 2121	05/02 0900	05/03 1702	04/30 0843	F	30 → 120	90	120 (320)	640 (670)	425	−215	14 (22)	2	2	3	irregular *Pt*
				05/01 2121	F	50 → 210	160									
				05/03 1702	F	15 → 53	38									
8	05/04 0203		05/05 0200	05/04 0203	F	47 → 127	80	220 (800)	770 (860)	540	−230	19 (42)	3	0	N	weak rotations of **B**
				05/04 0230	/	130 → 600	470									
9	06/02 1028	06/02 1028	06/02 1900					80	440	370	−70	12.3	1	N	2	
10[b]	06/24 1300	06/24 1300	06/26 1900	06/25 1543	F	70 → 160	90	178	535	395	−140	18		2, 0[n]	2	ACE[o], ICME + ICME, shock at the center
									505	460	−45					
11[b]	07/10 1939	07/10 1939	07/12 0514					150	405	333	72	17.3		0	Y	ACE
12[b]	07/12 0514	07/12 0514	07/13 1828					90	450	340	−110	14		N	N	ACE, closely following an ICME
13	08/10 0031	08/10 1320	08/12 1530	08/10 0031	F	20 → 70	50	100	455 (510)	350	−95	12.2	2	0	N	V_p irregular
14	08/19 1840	08/20 0900	08/21 1900	08/19 1840	F	27 → 77	50	135	350	287	−63	16.5	1	2	1	V_p irregular
15	08/26 0640	08/27 0530	08/28 0100	08/26 0640	F	40 → 306	266	110 (400)	710 (850)	530	−180	16 (25)	2	0	Y	T_p high, weak rotation of **B**
16	09/23 0400		09/23 1500					62	500	375	−125	9	3	1	N	weak rotations of **B**
17	09/24 2321	09/25 0600	09/26 1142	09/24 2321	F	110 → 800	690	160 (815)	860	580	−280	20 (40)	1	2	2	
18	10/02 0654		10/04 0900	10/02 0654	F	40 → 160	120	220	720	440	−280	19.6	3	N	N	ACE, weak rotations of **B**
19	10/18 1929	10/19 0425	10/20 0800	10/18 1929	F	45 → 140	95	280 (390)	435	360	−75	26	2	2	3	before an SIR

(*Continued on next page*)

APPENDIX
(*Continued*)

#	Start UT (mm/dd hhmm)	Start UT of magnetic obstacle[a] (mm/dd hhmm)	End UT (mm/dd hhmm)	Discontinuity UT	F/R[c] Shock	ΔP[d] (pPa)		P_{max} (pPa)	V_{max} (km s^{-1})	V_{min} (km s^{-1})	ΔV[e] (km s^{-1})	B_{max} (nT)	Group[f]	$C + R$[g]	Lepping[h]	Comments
20	10/23 1235		10/24 1800	10/23 1235	F	17 → 115	98	100	610	445	−165	13.2	3	0	N	ACE
21	11/07 2200	11/07 2200	11/10 2130	11/08 0422	F	140 → 500	360	580	640	400	−240	36.3	1	1, 2	1	ACE, ICME + ICME, shock at the center
									450	370	−80					
22	11/13 0000	11/13 0000	11/14 0700	11/13 0054	/	100 → 165	65	215	420	350	−70	20.5	2	2	Y	ACE, slow
23	11/30 0418	11/30 0900	12/01 0254	11/30 0418	F	25 → 100	75	140 (150)	490 (500)	420	−70	16.5	2	0	N	ACE, slow
24[b]	12/26 0956		12/27 0009	12/26 0956	F	52 → 105	53	110	550	400	−150	13	3	N	N	after an SIR
25	12/28 1735	12/29 0530	12/31 0100	12/28 1735	/	52 → 110	58	75 (130)	450	370	−80	12 (15.2)	2	0	N	ACE, slow, BDE
							1999									
1	01/22 1948	01/22 2330	01/23 1500	01/22 1948	F	60 → 123	63	190	680 (685)	540	−140	19 (20)	2	0	Y	ACE, BDEs
2[b]	02/18 0210	02/18 1000	02/20 1700	02/18 0210	F	40 → 385	345	320 (385)	680	400	−280	26 (29)	2	2	3	ACE
3	04/16 1036	04/16 1800	04/17 2000	04/16 1036	F	35 → 85	50	260	460 (470)	380	−80	24.6	1	2	3	ACE, *classic*
4	04/21 0423	04/21 0423	04/22 1823					50	560	430	−130	9.3	2	1	Y	ACE, *Wind* was in Earth's magnetosheath
5	05/28 2140	05/28 2140	05/30 1046					43	415	365	−50	8.5	2	N	N	strong rotations of **B**, V_p irregular and noisy
6[b]	06/26 0547		06/28 0600	06/26 0232	F	65 → 150	85	460	910	307	603	25		1, 0	N	ICME+SIR, V_p peaks in the center
				06/26 1932	F	120 → 395	275									
7	07/02 0026		07/05 1346	07/02 0026	F	16 → 54	38	93	680	380	−300	11.7	3	0	N	long, ACE
8	07/06 1417		07/07 1655	07/06 1417	F	20 → 58	38	75	510	400	−110	12	3	1	Y	ACE, possibly several flux ropes nearly in contact

(*Continued on next page*)

APPENDIX
(*Continued*)

#	Start UT (mm/dd hhmm)	Start UT of magnetic obstacle[a] (mm/dd hhmm)	End UT (mm/dd hhmm)	Discontinuity UT	F/R[c] Shock	ΔP[d] (pPa)		P_{max} (pPa)	V_{max} (km s^{-1})	V_{min} (km s^{-1})	ΔV[e] (km s^{-1})	B_{max} (nT)	Group[f]	$C+R$[g]	Lepping[h]	Comments
9[b]	07/07 2132	07/07 2132	07/09 0544	07/08 0400	F	20 → 45	25	73	450	320	−130	12	1	1	Y	
10	07/12 0122		07/13 1345	07/12 0122	F	50 → 115	65	130	322	282	−40	12.2	3	N	N	T_p not low
11[b]	07/30 1910		08/02 0600					285	670	420	−250	18.3 (24)		1, 1	N	ACE, might associated with the interaction of two CMEs from the Sun, causing compressions of **B** and T_p
12	08/04 0117		08/05 1230	08/04 0117	F	40 → 110	70	120	383	325	−58	14	3	N	N	ACE
13[b]	08/09 1018	08/09 1018	08/10 1840					103	385	314	−71	13.8	1	2	1	strong rotations, ICME + SIR
14[b]	08/21 1600		08/23 1035					50	510	380	−130	9.2		1	N	closely followed by an SIR
15	09/15 0720	09/15 0720	09/15 1942	09/15 0720	F	45 → 97	52	115	680	550	−130	16	1	1	Y	ACE
16[b]	09/22 1146		09/23 2042	09/22 1146	F	160 → 360	200	520	600	500	−100	31.3	3	0	Y	ACE, with SIR
17[b]	10/21 0221	10/21 0436	10/22 0650	10/21 0221	F	73 → 383	310	610	590	347	373	38		0	Y	ICME + SIR, *Pt* trough in the center, concave
18	11/12 1820	11/12 1820	11/14 0930	11/13 1214	F	23 → 67	44	120	487	400	−87	16	1	0, 1	Y	ACE
19[b]	11/22 0156		11/24 0640	11/21 1713	/	85 → 126	41	200	510	410	−100	16.3		0	Y	T_p, V_p irregular, SIR + ICME
20	12/12 1655	12/12 1655	12/13 1630	12/12 1515	F	12 → 70	58	105	760	440	−320	15	1	0	Y	ACE
21	12/14 0340	12/14 0340	12/16 0200					80	490	340	−150	11.5	2	0	Y	ACE, slow
22	12/26 2128		12/28 0447	12/26 2128	F	40 → 70	30	95	460	360	100	9.3 (13)	3	1	N	ACE

(*Continued on next page*)

APPENDIX
(*Continued*)

#	Start UT (mm/dd hhmm)	Start UT of magnetic obstacle[a] (mm/dd hhmm)	End UT (mm/dd hhmm)	Discontinuity UT	F/R[c] Shock	ΔP[d] (pPa)		P_{max} (pPa)	V_{max} (km s^{-1})	V_{min} (km s^{-1})	ΔV[e] (km s^{-1})	B_{max} (nT)	Group[f]	$C+R$[g]	Lepping[h]	Comments
							2000									
1	01/22 0023	01/22 1700	01/25 0820	01/22 0023	F	40 → 80	40	220	440	330	−110	18.6	1	1	Y	ACE, BDEs, slow ICME, T_p not low
2	02/11 0213		02/11 2300	02/11 0213	F	22 → 90	68	120	550	400	−150	12.5	3	0	N	ACE, BDE
3	02/11 2319	02/12 0715	02/13 0015	02/11 2319	F	30 → 270	240	280 (380)	600	510	−90	22.4 (25)	1	1	3	ACE, BDE
4	02/14 0657		02/15 1530	02/14 0657	F	27 → 75	48	93	690	480	−210	11	3	0	N	ACE
5	02/20 2100	02/21 0500	02/22 1200	02/20 2100	F	45 → 215	170	225	468	320	−148	18	2	2	3	
6	03/01 0330	03/01 0330	03/02 0300	03/01 0152	/	16 → 32	16	55	542	440	−102	10.5	2	0	N	
7	03/29 2330	03/29 2330	03/31 2000	03/31 0316	/	46 → 86	40	86	528	370	−158	9	1	0	Y	followed by SIR, weak but is Group 1
8	04/03 1356	04/04 0142	04/05 2035	04/03 1356	/	14 → 34	20	86	430	355	−75	12	1	N	N	ACE, slow ICME, BDE
9	04/06 1632	04/06 1632	04/08 0600	04/06 1632	F	50 → 480	430	520	630	515	−115	34	1	1	N	low T_p region after high Pt and **B** rotation region
				04/07 0912	/	65 → 22	−43									
10	05/07 0000	05/07 0000	05/08 2110					110	430	330	−100	15	1	0	N	V_p gradually declines, T_p not low
11	06/04 1450	06/05 0600	06/06 1630	06/04 1450	/	22 → 57	35	210	498 (550)	418	−80	17.5	1	1	N	not smooth
12	06/08 0905		06/09 1600	06/08 0905	F	70 → 450	380	450	800	590	−210	26	3	0	Y	
13	06/12 2200		06/14 0615	06/12 2200	/	30 → 115	85	150	580	415	−165	9.7	3	0	Y	weak
14	06/23 1228		06/25 1922	06/23 1228	F	42 → 275	227	310	600	405	−195	23	3	0	3	ACE, BDE
15	07/01 0100	07/01 0100	07/02 1829					70	440	360	−80	9.7	1	1	2	ACE, no BDE

(*Continued on next page*)

APPENDIX
(*Continued*)

#	Start UT (mm/dd hhmm)	Start UT of magnetic obstacle[a] (mm/dd hhmm)	End UT (mm/dd hhmm)	Discontinuity UT	F/R[c] Shock	ΔP[d] (pPa)		P_{max} (pPa)	V_{max} ($km\,s^{-1}$)	V_{min} ($km\,s^{-1}$)	ΔV[e] ($km\,s^{-1}$)	B_{max} (nT)	Group[f]	$C + R$[g]	Lepping[h]	Comments
16	07/11 1124		07/13 0222	07/11 1124	F	95 → 300	205	310	540	465	−75	22	3	1	Y	ACE, *Wind* was around bow shock
17	07/13 0919		07/14 0400	07/13 0919	F	140 → 420	280	420	680	580	−100	27	3	0	N	ACE, Wind was in the magnetosheath, small $\|\Delta V\|$
				07/13 0936	/	280 → 400	120									
18	07/14 1500	07/14 1500	07/15 1400	07/14 1500	F	shock identified by magnetic coplanarity only						18		1	2	plasma data gap from ACE, data gap (07/14 – 07/17) of *Wind*
19	07/15 1416	07/15 1900	07/17 0100	07/15 1416	F	ditto						58		2	2	plasma data gap, LARGE B
20	07/19 1449		07/21 1927	07/19 1449	F	22 → 70	48	120	650	460	−190	13.8	3	0	Y	ACE
21[b]	07/26 1755		07/27 1953	07/26 1755	F	43 → 77	34	130	400	330	−70	11	3	1	Y	ACE, several ICMEs nearby
22[b]	07/28 0543		07/29 0910	07/28 0543	F	40 → 240	200	460	485	390	−95	26	3	2	2	ACE
				07/28 0910	F	133 → 460	327									
23[b]	08/10 0408	08/10 1920	08/11 1800	08/10 0408	F	30 → 95	65	80 (125)	445	390	−55	13.5 (15)	2	2	Y	ACE, weak
24[b]	08/11 1812	08/12 0446	08/13 2210	08/11 1812	F	50 → 200	150	475	630 (680)	537	−93	35	1	2	1	ACE
25	09/02 1200	09/02 1200	09/03 1215					68	460	400	−60	11	1	0	Y	ACE, weak, BDE in first half day of 09/03
26	09/04 1245	09/04 2145	09/06 0043	09/04 1245	F	20 → 60	40	60	430 (490)	350	−80	10.5	2	N	N	ACE, BDE

(*Continued on next page*)

APPENDIX
(*Continued*)

#	Start UT (mm/dd hhmm)	Start UT of magnetic obstacle[a] (mm/dd hhmm)	End UT (mm/dd hhmm)	Discontinuity UT	F/R[c] Shock	ΔP[d] (pPa)		P_{max} (pPa)	V_{max} (km s^{-1})	V_{min} (km s^{-1})	ΔV[e] (km s^{-1})	B_{max} (nT)	Group[f]	$C+R$[g]	Lepping[h]	Comments
27	09/06 1615	09/06 2300	09/10 0400	09/06 1615	F	60 → 225	165	280	520	360	−160	20	3	N	N	ACE
28	09/17 1409	09/17 2320	09/19 0625					710	870	625	−245	41	3	2	3	ACE, noisy *Wind* data
29	10/03 0102	10/03 1700	10/04 1230	10/03 0102	F	40 → 93	53	190	442 (488)	385	−57	18	1	2	1	irregular *Pt*
30	10/05 0329	10/05 1100	10/06 0600	10/05 0329	F	35 → 205	170	420	535	500	−35	29	3	1	N	fast ICME
31	10/12 2233	10/13 0600	10/14 0716	10/12 2233	F	30 → 173	143	290	490	385	−105	20	1	2	2	
32	10/28 0932	10/28 2230	10/29 2330	10/28 0932	F	70 → 215	145	190 (250)	415	342	−73	18.2	3	2	3	
33	11/06 0930	11/06 2230	11/08 0325	11/06 0930	F	15 → 75	60	264	615	430	−185	25	1	2	2	
				11/08 1404	R	70 → 23	−47									
34	11/10 0620		11/10 1800	11/10 0620	F	100 → 1200	1100	2100	960	860	−100	32	3	N	N	too high T_p and *Pt*, big CME from the Sun, data gap of ACE, BDEs
35	11/11 0413		11/11 2100	11/11 0413	F	20 → 73	53	140	970	730	−240	12	3	0	N	
36	11/28 0458	11/28 1131	11/30 0800	11/28 0458	F	32 → 95	63	143	497	460	−37	16.3	1	1	N	ACE, complex, shock around the center
				11/29 0307	F	55 → 100	45									
				11/29 0523	F	80 → 130	50									
37	12/03 0321		12/05 0800	12/03 0321	F	32 → 62	30	90	497	320	−177	12.7	3	N	N	ACE, weak, five-hour BDE
							2001									
1	01/13 0227		01/14 0000	01/13 0227	F	22 → 123	101	123	450	378	−72	16	3	N	N	BDE from 01/13 0900
2	01/23 1007		01/26 0748	01/23 1007	F	20 → 135	115	160	565	338	−227	13.5	3	1	N	ACE, BDEs
3	01/31 0837		02/01 1530	01/31 0837	F	30 → 143	113	155	485	395	−90	14.5	3	N	N	

(*Continued on next page*)

APPENDIX
(*Continued*)

#	Start UT (mm/dd hhmm)	Start UT of magnetic obstacle[a] (mm/dd hhmm)	End UT (mm/dd hhmm)	Discontinuity UT	F/R[c] Shock	ΔP^{d} (pPa)		P_{max} (pPa)	V_{max} (km s^{-1})	V_{min} (km s^{-1})	ΔV^{e} (km s^{-1})	B_{max} (nT)	Group[f]	$C+R^{g}$	Lepping[h]	Comments
4[b]	03/04 0500	03/04 0500	03/05 0140					83	470	400	−70	13		0	N	in an SIR, no BDE
5	03/19 1134	03/19 1900	03/22 0000	03/19 1134	F	53 → 160	107	175 (218)	465	290	−175	20 (21)	1	2	1, 3	classic
6	03/27 0202		03/27 1009	03/27 0202	/	30 → 125	95	183	445	390	−55	18	3	N	N	data gap around 03/27 0202, followed closely by another ICME
7	03/27 1807	03/27 2257	03/28 1345	03/27 1807	F	90 → 310	220	180 (410)	650	565	−85	19 (28)	2	0	N	V_p irregular
8	03/31 0023		03/31 2138	03/31 0023	F	100 → 2100	2000	2100	770	500	−270	70	3	1	N	
9[b]	03/31 2140	04/01 0421	04/03 0310	03/31 2140	/	170 → 400	230	50 (460)	830	515	−315	10 (35)		0	N	ACE, no BDE, closely following an ICME
				03/31 2256	R	450 → 230	−220									
10	04/04 1423	04/04 1800	04/05 0545	04/04 1423	F	20 → 200	180	275	800	650	−150	23	3	0	1	*Wind* data gap (04/06 – 04/30), ACE, BDE
11	04/07 1700		04/08 0551	04/07 1700	F	30 → 115	85	160	560	460	−100	15.5	3	N	N	ACE, BDE, T_p not low
12	04/08 1032		04/10 0900	04/08 1032	F	30 → 320	290	345	800	520	−280	22	3	0	N	ACE, BDE
13	04/11 1315	04/11 2212	04/13 0446	04/11 1315	F	30 → 130	100	550 (950)	740	600	−140	35 (41)	1	2	2	ACE, half period with high T_p, two shocks close to each other
				04/11 1453	/	150 → 230	80									
				04/11 1528	F	260 → 600	340									
14	04/13 0707	04/13 1030	04/14 1010	04/13 0707	F	12 → 45	33	105	830	600	−230	15		0	N	ACE, BDE
15	04/18 0005		04/20 1100	04/18 0005	F	20 → 200	180	360	530	370	−160	25	3	0	N	ACE, BDE

(*Continued on next page*)

APPENDIX
(*Continued*)

#	Start UT (mm/dd hhmm)	Start UT of magnetic obstacle[a] (mm/dd hhmm)	End UT (mm/dd hhmm)	Discontinuity UT	F/R[c] Shock	ΔP^d (pPa)		P_{max} (pPa)	V_{max} (km s^{-1})	V_{min} (km s^{-1})	ΔV^e (km s^{-1})	B_{max} (nT)	Group[f]	$C+R^g$	Lepping[h]	Comments
16	04/21 1508	04/21 2335	04/23 0030	04/21 1508	F	16 → 46	30	120	390	330	−60	15.5	1	2	1	ACE, no obvious BDE
17	04/28 0432	04/28 1550	04/29 1400	04/28 0432	F	60 → 400	340	170 (400)	720 (750)	560	−160	19 (25.5)	2	2	2	ACE, V_p classic, short interval of BDE
18	05/27 1447	05/28 0430	05/29 1030	05/27 1447	F	20 → 95	75	106	560 (640)	415	−145	10 (15)	1	2	1	
19	06/27 0300	06/27 0300	06/28 1700					24	480	363	−117	3.5		0	N	ACE, *Pt* very small, in a declining stream
20	07/09 0300	07/09 0300	07/12 0300					73	482	320	−162	9.2		1	2	*Pt* trough, slow, before an SIR
21	08/03 0719		08/03 1815	08/03 0719	F	32 → 180	148	210	465	410	−55	12	3	0	N	a short interval with BDEs
22[b]	08/05 0115	08/05 0115	08/05 2345	08/05 1156	F	53 → 93	40	95	500	370	−130	13.7		N	N	ACE, with an SIR, BDE
23	08/17 1102	08/17 2000	08/18 2000	08/17 1102	F	20 → 210	190	430 (500)	600	470	−130	31	2	0	N	
24	08/27 1938		08/28 1650	08/27 1938	F	40 → 280	240	300	600	500	−100	19	3	0	N	BDE
25	09/17 2145		09/19 1747					110	480	400	−80	12		N	N	ACE, plot of *Pt* looks like SIR, big deflection of V_p, BDE occurred during a part of the interval
26	09/25 2018		09/27 0400	09/25 2018	F	50 → 310	260	550	740	460	−280	32.6	3	N	N	data gap of ACE
27[b]	09/29 0906	09/29 1130	09/30 1600	09/29 0906	F	30 → 80	50	110	725	460	−265	14.5	1	1	N	ACE
28[b]	09/30 1847	09/30 2200	10/01 1600	09/30 1847	F	55 → 165	110	175 (200)	560	440	−120	20	3	0	N	ACE

(*Continued on next page*)

APPENDIX
(*Continued*)

#	Start UT (mm/dd hhmm)	Start UT of magnetic obstacle[a] (mm/dd hhmm)	End UT (mm/dd hhmm)	Discontinuity UT	F/R[c] Shock	ΔP[d] (pPa)		P_{max} (pPa)	V_{max} (km s^{-1})	V_{min} (km s^{-1})	ΔV[e] (km s^{-1})	B_{max} (nT)	Group[f]	$C+R$[g]	Lepping[h]	Comments
29[b]	10/02 2324	10/02 2324	10/03 1630	10/03 0807	F	122 → 142	20	240	600	460	140	23.8	1	2	N	ACE, followed by another ICME
30[b]	10/03 2200		10/04 0700					85	590	470	120	12	3	N	N	ACE, following a leading ICME
31	10/21 1614	10/22 0043	10/22 2310	10/21 1614	F	70 → 400	330	160 (500)	680	500	−180	18 (30)	2	0	N	ACE, low T_p, **B** irregular and noisy, BDE for whole interval
				10/22 0013	R	260 → 120	−140									
32	10/28 0243		10/31 1254	10/28 0243	F	33 → 190	157	230	525	325	−200	22	3	0	N	ACE
33	10/31 1348	10/31 2100	11/02 1200	10/31 1348	F	12 → 70	58	93 (113)	400	305	−95	13.6	1	2	3	V_p noisy and irregular
34	11/05 1931		11/06 2017									80		1	N	ACE, plasma data gap, same to *Wind*
35	11/14 0800		11/15 0900									4.6		N	N	ACE, plasma data gap, same to *Wind*
36	11/15 1800	11/15 1800	11/16 1030					180	380	325	55	16.3		N	N	ACE, plasma data gap (11/14 1200 – 11/15 1700)
37	11/19 1736		11/20 1700	11/19 1736	F	30 → 120	90	140	580	405	−175	13.5	3	1	N	some data gaps during 11/01 – 11/16, taking five days off, ACE, BDE
38	11/24 0552	11/24 1545	11/25 1638	11/24 0552	F	100 → 1400	1300	210 (1900)	970	600	−370	23 (58)	2	2	3	very strong, ACE data gap (11/24 0420 – 1730)

(*Continued on next page*)

APPENDIX
(*Continued*)

#	Start UT (mm/dd hhmm)	Start UT of magnetic obstacle[a] (mm/dd hhmm)	End UT (mm/dd hhmm)	Discontinuity UT	F/R[c] Shock	ΔP[d] (pPa)		P_{max} (pPa)	V_{max} (km s^{-1})	V_{min} (km s^{-1})	ΔV[e] (km s^{-1})	B_{max} (nT)	Group[f]	$C+R$[g]	Lepping[h]	Comments
				11/24 1400	R	580 → 180	−400									
39[b]	12/29 0449	12/30 0021	12/30 1820	12/29 0449	F	50 → 290	240	200 (460)	430 (510)	350	80	20.8 (24.7)	2	1	N	ACE, followed by another ICME
40[b]	12/30 1933		12/31 0747	12/30 1933	F	80 → 380	300	440	700	510	190	27	3	N	N	ACE, weak rotations, BDE
							2002									
1	02/28 0507	02/28 1835	03/01 0900	02/28 0507	F	50 → 240	190	140	420	360	−60	14.6	1	1	N	V_p irregular
2	03/18 1315		03/20 0938	03/18 1315	F	50 → 350	300	600	480	330	−120	22.5	3	2	2	T_p not low
3	03/20 1320		03/22 0300	03/20 1320	/	80 → 188	108	350	616	415	−201	21	3	0	N	
4[b]	03/23 1125	03/24 1200	03/25 2100	03/23 1125	F	22 → 81	59	180	490 (520)	410	−80	21	1	2	2	V_p irregular, followed by an SIR
				03/25 0115	F	105 → 180	75									
5	04/14 1149	04/14 1149	04/15 1800	04/14 1149	/	43 → 73	30	90	440	332	−108	11	2	N	N	ACE, BDE
6	04/17 1102		04/19 0825	04/17 1102	F	100 → 800	700	900	640	430	−210	33	3	2	1	followed by another shock
7	04/19 0827	04/20 0045	04/21 1630	04/19 0827	F	50 → 235	185	200 (265)	650	440	−210	21.5 (23.7)	1	2	3	
8	04/23 0415		04/24 1700	04/23 0415	F	40 → 275	235	310	650	472	−198	17	3	N	N	ACE, T_p high
9	05/10 1114		05/11 1000	05/10 1114	/	40 → 110	70	180	418	330	−88	15.5	3	N	N	
10[b]	05/11 1030		05/11 2350	05/11 1030	F	60 → 270	210	320	470	400	−70	23	3	0	N	ICME (05/11 1618 ~ 05/12 0100, T_p not low) + SIR
				05/12 0234	/	48 → 24	−24									
11	05/18 1920	05/19 0240	05/20 0257	05/18 1920	F	37 → 270	233	208 (370)	475 (500)	380	−95	20	2	N	1	ACE
12	05/20 0335		05/21 2100	05/20 0335	F	38 → 103	65	148	533	370	−163	16	3	0	N	

(*Continued on next page*)

APPENDIX
(*Continued*)

#	Start UT (mm/dd hhmm)	Start UT of magnetic obstacle[a] (mm/dd hhmm)	End UT (mm/dd hhmm)	Discontinuity UT	F/R[c] Shock	ΔP[d] (pPa)		P_{max} (pPa)	V_{max} (km s^{-1})	V_{min} (km s^{-1})	ΔV[e] (km s^{-1})	B_{max} (nT)	Group[f]	$C + R$[g]	Lepping[h]	Comments
13	05/23 1016		05/25 1820	05/23 1016	F	150 → 550	400	1400	975	360	−615	54	3	2	3	ACE, strong, BDE
14	07/17 1526		07/19 0730	07/17 1526	F	50 → 300	250	260	540	408	−132	19.5	3	0	N	ACE, BDE
15[b]	07/19 0932	07/19 0932	07/21 1108	07/19 0932	F	18 → 85	67	200	925	480	−445	20	1	0	N	classic SIR + ICME, ACE, BDE, V_p big deflections
				07/19 1443	F	50 → 110	60									
16	07/25 1300		07/26 1830	07/25 1300	F	40 → 85	45	100	550	420	−130	13.8	3	N	N	ACE, T_p not low, BDE
17	07/29 1242		07/30 1800	07/29 1242	F	23 → 90	67	150	570	400	−170	17.5	3	N	N	ACE
18	08/01 0425	08/01 0425	08/01 2220	08/01 0425	F	30 → 100	70	120	463	430	−33	15	1	2	3	ACE, followed by another ICME
19	08/01 2220	08/02 0422	08/03 0526	08/01 2220	F	45 → 125	80	80 (130)	525	407	−118	13.5 (16)	1	2	2	ACE
20	08/18 1810		08/21 2115	08/18 1810	F	13 → 140	127	200	600	370	−230	16.7	3	1	N	ACE
21	08/26 1115		08/26 2300	08/26 1115	F	50 → 160	110	230	430	355	−75	17	3	N	N	
				08/26 1121	SF[p]	160 → 120	−40									
22[b]	09/07 1622		09/08 2000	09/07 1622	F	30 → 250	220	290	620	450	−165	23	3	0	N	ICME + ICME
23[b]	09/08 2225	09/08 2225	09/10 2000					60	552	385	−167	10	2	0	N	
24	09/19 0617		09/20 2235	09/19 0617	/	30 → 60	30	90	780	370	−410	10.2	3	0	N	
25[b]	09/30 0755	09/30 2200	10/01 1430	09/30 0755	F	140 → 360	220	300	430	350	80	26.5	1	2	3	ICME in SIR
26	10/02 2241	10/02 2241	10/04 1900	10/02 2241	F	14 → 36	22	100	543	370	−173	14	2	2	N	
27	11/16 2304	11/17 0722	11/18 2346	11/16 2304	F	37 → 67	30	90	510	380	−100	11.3	2	2	N	ACE, bad
28	11/26 2110		11/27 2015	11/26 2110	F	60 → 440	380	510	600	500	−100	29	3	N	N	ACE
						2003										
1	02/01 1313	02/01 2131	02/03 0447	02/01 1313	/	45 → 67	22	120	700	470	−230	13.5	2	0	N	

(*Continued on next page*)

APPENDIX
(*Continued*)

#	Start UT (mm/dd hhmm)	Start UT of magnetic obstacle[a] (mm/dd hhmm)	End UT (mm/dd hhmm)	Discontinuity UT	F/R[c] Shock	ΔP[d] (pPa)		P_{max} (pPa)	V_{max} (km s^{-1})	V_{min} (km s^{-1})	ΔV[e] (km s^{-1})	B_{max} (nT)	Group[f]	$C + R$[g]	Lepping[h]	Comments
2	02/17 2151		02/19 0044	02/17 2151	/	40 → 70	30	156	700	570	−130	16.2		0	N	ACE, high **B** in the leading region, no BDE, followed by an SIR
3	03/20 0421	03/20 0830	03/20 2230	03/20 0421	F	45 → 107	62	85 (120)	810 (840)	605	−205	12.8 (15.5)	2	2	1	ACE, no BDE
4	05/09 0456	05/09 0800	05/10 0600	05/09 0456	F	22 → 85	63	90 (120)	900	650	−250	12.2	2	1	N	ACE, no BDE
5	05/29 1152	05/29 1300	05/29 1830	05/29 1152	F	17 → 58	41	105	680 (690)	640	−40	16	2	1	N	ACE, BDE, closely followed by an ICME
6	05/29 1830	05/30 0119	05/30 1415	05/29 1830	F	130 → 500	370	450 (750)	665 (800)	550	−115	30 (36)	2	1	N	ACE, BDE
7	05/30 1553		05/31 1125	05/30 1553	/	70 → 225	155	250	850	660	−190	22	3	0	N	ACE, weak, large **B** in the leading part, BDE
8	06/15 0617	06/15 0617	06/16 2100					110	600	440	−160	15	1	1	N	ACE, weak rotations of **B**, *Pt* mimics SIR
9[b]	06/17 0030	06/17 0030	06/18 0900	06/18 0442	F	70 → 143	73	170	540	442	−98	19	1	2	3	closely followed by an ICME
10	07/06 1225		07/07 1142	07/06 1225	F	22 → 55	33	70	720	480	−240	9.5	3	0	N	ACE, no BDE, T_p not low
11	07/23 1400		07/24 1400					50	515	395	120	9		1	N	ACE, *Pt* irregular
12[b]	08/04 1930	08/04 1930	08/05 2300					95	512	410	−102	12.5	2	1	N	bad rotation, before an SIR
13	08/18 0113	08/18 0113	08/19 1623	08/17 1341	F	50 → 212	162	172 (240)	500 (530)	400	−100	20 (23)	1	2	2	ACE, T_p disturbance
14	10/21 2300	10/21 2300	10/24 0228	10/21 1938	/	45 → 65	20	95	760	410	−350	12	1	1	N	ACE

(*Continued on next page*)

APPENDIX
(*Continued*)

#	Start UT (mm/dd hhmm)	Start UT of magnetic obstacle[a] (mm/dd hhmm)	End UT (mm/dd hhmm)	Discontinuity UT	F/R[c] Shock	ΔP^{d} (pPa)		P_{max} (pPa)	V_{max} (km s^{-1})	V_{min} (km s^{-1})	ΔV^{e} (km s^{-1})	B_{max} (nT)	Group[f]	$C+R^{g}$	Lepping[h]	Comments
15	10/24 1449		10/25 1123	10/24 1449	F	70 → 400	330	670	605	510	−95	34	3	1	N	ACE, T_p not low, because of interaction of several ICMEs
16	10/26 0810		10/28 0130	10/26 0810	F	37 → 62	25	133	600	420	−180	17		1	N	ACE, *Pt* irregular
				10/26 1833	F	60 → 120	60									
17	10/29 0842	10/29 0842	10/30 1000									48		2	N	ACE, plasma data gap (10/28 1300 – 10/31 0100), Halloween event
18	10/31 0127	10/31 0127	11/01 1720					700	1200	600	−600	40		1	N	
19	11/04 0600		11/04 1530	11/04 0600	F	50 → 460	410	500	770	700	−70	27.5	3	N	N	ACE
20	11/06 1920		11/08 0430	11/06 1920	F	20 → 120	100	150	600	410	−190	14.5	3	N	N	ACE
21	11/15 0519		11/15 1700	11/15 0519	F	32 → 190	158	195	730	620	−110	14	3	N	N	ACE, BDEs
22	11/20 0728	11/20 1000	11/21 0615	11/20 0728	F	60 → 345	285	1250	720	520	−200	56	1	2	N	ACE, strong, *CLASSIC*
						2004										
1	01/09 1451		01/12 1300	01/09 1451	/	50 → 110	60	165	700	480	−220	15.5	3	1	/	ACE, 16-h low T_p
2	01/22 0105		01/23 0700	01/22 0105	F	40 → 420	380	420	700	520	−120	29	3	0	/	big shock, ACE, BDE
3	01/23 1421	01/23 1421	01/25 0300	01/23 1421	/	27 → 71	44	80	560	460	−100	13	2	1	/	ACE, small $\lvert B \rvert$, BDE, closely following an ICME
4[b]	04/03 0955	04/04 0110	04/05 1932	04/03 0955	/	28 → 58	30	170	525	370	−155	19.3	1	2	/	classic, followed by an SIR

(*Continued on next page*)

APPENDIX
(*Continued*)

#	Start UT (mm/dd hhmm)	Start UT of magnetic obstacle[a] (mm/dd hhmm)	End UT (mm/dd hhmm)	Discontinuity UT	F/R[c] Shock	ΔP[d] (pPa)		P_{max} (pPa)	V_{max} (km s^{-1})	V_{min} (km s^{-1})	ΔV[e] (km s^{-1})	B_{max} (nT)	Group[f]	$C+R$[g]	Lepping[h]	Comments
				04/03 1422	/	50 → 80	30									
5	04/10 1927		04/11 1220	04/10 1927	F	20 → 85	65	110	520	405	−105	12.2	3	N	/	ACE, BDEs, but weak rotations of |**B**|, T_p not low
6	04/12 1736		04/13 0500	04/12 1736	F	25 → 90	65	120	510	440	−70	14	3	N	/	ACE, T_p not low, six-hour BDEs in the leading part
7	04/26 1518	04/26 1518	04/27 0925	04/26 1518	/	17 → 44	27	54	505	440	−65	8.5		1	/	ACE, low T_p, Pt irregular and weak, no BDEs, Wind was in magnetosphere
8	04/30 1600	04/30 1600	05/02 2100					62	460	370	−90	9.7	2	0	/	ACE, BDEs
9	07/22 0955	07/22 1335	07/23 0855	07/22 0955	F	20 → 95	75	175	700	450	250	19.6	2	1	/	ACE, with SIR
10	07/24 0531	07/24 1205	07/25 1535	07/24 0531	F	50 → 230	180	300	640	460	−180	25	2	2	/	V_p irregular, BDEs, among several ICMEs
				07/24 1153	/	150 → 260	110									
11	07/25 1734		07/26 1748					73	700	600	−100	13		1	/	ACE, BDEs, among several ICMEs
12	07/26 2229	07/27 0140	07/27 1532	07/26 2229	F	30 → 210	180	265	1025	800	−225	26.3	1	2	/	ACE, BDEs
13[b]	08/29 0908	08/29 0908	08/30 2020	08/29 0908	/	16 → 42	26	95	450	375	−75	14	1	2	/	V_p irregular, half a rotation of **B**
14	09/13 1945		09/14 2130	09/13 1945	F	60 → 360	300	400	645	520	−125	30	3	1	/	high T_p, V_p doesn't deline well, BDE
15	09/18 1210	09/18 1210	09/20 0800	09/18 1210	/	24 → 38	14	72	443	370	−73	9.8		1	/	overexpand[q], BDEs

(*Continued on next page*)

APPENDIX
(*Continued*)

#	Start UT (mm/dd hhmm)	Start UT of magnetic obstacle[a] (mm/dd hhmm)	End UT (mm/dd hhmm)	Discontinuity UT	F/R[c] Shock	ΔP[d] (pPa)		P_{max} (pPa)	V_{max} (km s^{-1})	V_{min} (km s^{-1})	ΔV[e] (km s^{-1})	B_{max} (nT)	Group[f]	$C+R$[g]	Lepping[h]	Comments
16	09/22 0554		09/22 1838	09/22 0554	F	40 → 96	56	115	550	460	−90	11	3	N	/	ACE, T_p not low, BDEs
17	11/09 1821	11/09 2028	11/11 0632	11/09 0914	F	15 → 105	90	700	815	550	−265	41	1	2	/	several SIRs in October, no ICME; ACE, in the fast stream, BDE, maybe a slow reverse shock[p] at 20:26:30
				11/09 1821	F	100 → 420	320									
18	11/11 1649		11/13 1100	11/11 1649	F	20 → 75	55	192	720	470	−140	18	3	1	/	BDE
				11/11 2120	/	42 → 160	118									
19	12/11 1257	12/12 2230	12/14 0238	12/11 1257	F	20 → 95	75	103 (120)	400 (590)	370	−30	15.7	2	0	/	ACE, BDE
20	12/27 0448		12/28 1800	12/27 0448	/	48 → 65	17	90	580	405	−175	10.3	3	1	/	ACE, BDE, *Pt* irregular, maybe a slow forward shock at 12/27 04:48

[a]For most Group 3 ICMEs, the spacecraft do not traverse some part of magnetic obstacle, so that the start time of obstacle is not given for such events. The stop time of the magnetic obstacle, not given in the survey, is the same as the end time of the ICME event.
[b]Hybrid event consisting of not only one event.
[c]F/R Shock: forward/reverse shock.
[d]ΔP: instant change in total prependicular pressure across the discontinuity, in the unit of pico-Pascal (pPa), and "/" means neither a forward shock nor a reverse shock.
[e]ΔV: change in solar wind velocity during one event; negative value indicates that the solar wind velocity declines through the event.
[f]Group: classification of ICME into three groups depending on the behavior of *Pt*.

(Continued on next page)

[g] $C + R$: from the list of Cane and Richardson (2003) and private communication in 2006; "/" means the data in 1995 is unavailable; 0 – 2 is their magnetic cloud (MC) index: 0 indicates that the field shows little evidence of rotation; 1 suggests evidence of a relatively organized field rotation within the ICME, but not a MC; 2 is the MC which can be modeled by a force-free flux rope.
[h] Lepping: *Wind*_MC list of R. P. Lepping (*http://lepmfi.gsfc.nasa.gov/mfi/mag_cloud_pub1.html*); "/" means the 2004 data is unavailable; 1 – 3 is the rising quality of MC; "Y" indicates that the event is also in the ACE list of CME, MC and complex ejecta from Oct, 1997 to 2000 (*http://www.bartol.udel.edu/~chuck/ace/ACElist/obs_list.html*).
[i] N: not an ICME in the corresponding list.
[j] (): the value in the "magnetosheath" region.
[k] FF: fast forward shock.
[l] From Larson's shock list (*http://sprg.ssl.berkeley.edu/~davin/IPShocks.html*).
[m] For the ICME, two events in $C + R$ list, however, only one CME from the Sun is observed from Large Angle and Spectrometric Coronagraph (LASCO) (Brueckner *et al.*, 1995). Even if there are two ICMEs, they interact too closely, hardly separate them. On the other hand, it can arise from the interaction of two distorted parts of one CME.
[n] This ICME corresponds to two events in $C + R$ list, however, it is hard to separte them, because of the close interaction and the continous variations of B. Hence, we record it as one hybrid event, with two steps of variation of solar wind velocity specifically listed.
[o] ACE: from the ACE data.
[p] From Kasper's shock list (*http://space.mit.edu/home/jck/shockdb/shockdb.html*).
[q] Overexpansion: CME where the expansion is driven by a quite high initial internal pressure (Gosling *et al.*, 1994).

References

Bame, S.J., Asbridge, J.R., Feldman, W.C., Fenimore, E.E., and Gosling, J.T.: 1979, *Solar Phys.* **62**, 179.

Brueckner, G.E., *et al.*: 1995, *Solar Phys.* **162**, 357.

Burlaga, L.F.: 1991, in R. Schwenn and E. Marsch (eds.), *Physics of the Inner Heliosphere II*, Springer-Verlag, Berlin, p. 1.

Burlaga, L.F., Sittler, E., Mariani, F., and Schwenn, R.: 1981, *J. Geophys. Res.* **86**, 6673.

Cane, H.V. and Richardson, I.G.: 2003, *J. Geophys. Res.* **108**(A4), 1156, doi: 10.1029/2002JA009817.

Cane, H.V., Richardson, I.G., and St. Cyr, O.C.: 2000, *Geophys. Res. Lett*. **27**, 3591.

Feldman, W.C., Asbridge, J.R., Bame, S.J., and Montgomery, M.D.: 1973, *J. Geophys. Res.* **78**(19), 3697.

Feldman, W.C., Anderson, R.C., Asbridge, J.R., Bame, S.J., Gosling, J.T., and Zwickl, R.D.: 1982, *J. Geophys. Res.* **87**, 632.

Feldman, W.C., Anderson, R.C., Bame, S.J., Gosling, J.T., Zwickl, R.D., and Smith, E.J.: 1983, *J. Geophys. Res.* **88**, 9949.

Goldstein, R., Neugebauer, M., and Clay, D.: 1998, *J. Geophys. Res.* **103**, 4761.

Gosling, J.T.: 1990, in C.T. Russell, E.R. Priest, and L.C. Lee (eds.), *Physics of Magnetic Flux Ropes*, *Geophys. Monogr. Ser.*, AGU, Washington, DC, **58**, p. 343.

Gosling, J.T.: 1997, in N. Crooker, J.A. Joselyn, and J. Feynman (eds.), *Coronal Mass Ejections*, *Geophys. Monogr. Ser.*, AGU, Washington, DC, **99**, p. 9.

Gosling, J.T. and Pizzo, V.J.: 1999, *Spa. Sci. Rev*. **89**, 21.

Gosling, J.T., Birn, J., and Hesse, M.: 1995, *Geophys. Res. Lett.* **22**, 869.

Gosling, J.T., Pizzo, V., and Bame, S.J.: 1973, *J. Geophys. Res.* **78**, 2001.

Gosling, J.T., Hildner, E., MacQueen, R.M., Munro, R.H., Poland, A.I., and Ross, C.L.: 1976, *Solar Phys.* **48**, 389.

Gosling, J.T., Baker, D.N., Bame, S.J., Feldman, W.C., Zwickl, R.D., and Smith, E.J.: 1987, *J. Geophys. Res.* **92**, 8519.

Gosling, J.T., Bame, S.J., Feldman, W.C., McComas, D.J., Phillips, J.L., and Goldstein, B.E.: 1993, *Geophys. Res. Lett*. **21**, 2335.

Gosling, J.T., McComas, D.J., Phillips, J.L., Weiss, L.A., Pizzo, V.J., Goldstein, B.E., and Forsyth, R.J.: 1994, *Geophys. Res. Lett*. **21**, 2271.

Gosling, J.T., McComas, D.J., Phillips, J.L., Pizzo, V.J., Goldstein, B.E., Forsyth, R.J., and Lepping, R.P.: 1995, *Geophys. Res. Lett.* **22**, 1753.

Hirshberg, J. and Colburn, D.S.: 1969, *Planet Spa. Sci.* **17**, 1183.

Hirshberg, J., Bame, S.J., and Robbins, D.E.: 1972, *Solar Phys.* **23**, 467.

Hundhausen, A.J.: 1988, in V.J. Pizzo, T.E. Holzer, and D.G. Sime (eds.), *Proceedings of the Sixth International Solar Wind Conference*, *Tech. Note NCAR/TN-306+Proc*, **181**, Natl. Cent. Atmos. Res., Boulder, CO.

Hundhausen, A.J.: 1993, *J. Geophys. Res.* **98**, 13177.

Hundhausen, A.J.: 1999, in K.T. Strong, J.L.R. Saba, B.M. Haisch, and J.T. Schmelz (eds.), *The Many Faces of the Sun: A Summary of the Results from NASA's Solar Maximum Mission*, Springer, New York, p. 143.

Ipavich, F.M., Galvin, A.B., Gloeckler, G., Hovestadt, D., Bame, S.J., Klecker, B., Scholer, M., Fisk, L.A., and Fan, C.Y.: 1986, *J. Geophys. Res.* **91**, 4133.

Issautier, K., Perche, C., Hoang, S., Lacombe, C., Maksimovic, M., Bougeret, J.-L., and Salem, C.: 2005, *Advances in Spa. Res.* **35**, 2141.

Jian, L., Russell, C.T., Gosling, J.T., and Luhmann, J.G.: 2005a, *AGU*, Abstr. Spring, SH52A-11.

Jian, L., Russell, C.T., Gosling, J.T., and Luhmann, J.G.: 2005b, in B. Fleck, T.H. Zurbuchen, and H. Lacoste (eds.), *Proc. Solar Wind 11-SOHO 16, Connecting Sun and Heliosphere*, ESA, Noordwijk, The Netherlands, p. 731.

Jian, L., Russell, C.T., Luhmann, J.G, and Skoug, R.M.: 2006, *Solar Phys.*, in press.

Kahler, S.: 1988, in V.J. Pizzo, T.E. Holzer, and D.G. Sime (eds.), *Proceedings of the Sixth International Solar Wind Conference*, *Tech. Note NCAR/TN-306+Proc*, **181**, Natl. Cent. Atmos. Res., Boulder, CO, p. 215.

Klein, L.W. and Burlaga, L.F.: 1982, *J. Geophys. Res*. **87**, 613.

Lepping, R.P., Jones, J.A., and Burlaga, L.F.: 1990, *J. Geophys. Res*. **95**, 11957.

Lepping, R. P., *et al.*: 1995, *Spa. Sci. Rev.* **71**, 207.

Lepri, S.T., Zurbuchen, T.H., Fisk, L.A., Richardson, I.G., Cane, H.V., and Gloeckler, G.: 2001, *J. Geophys. Res*. **106**, 29231.

Lin, R.P., *et al.*: 1995, *Spa. Sci. Rev.* **71**, 125.

Lindsay, G.M., Russell, C.T., Luhmann, J.G., and Gazis, P.: 1994, *J. Geophys. Res*. **99**(A1), 11.

Linker, J.A., Mikic, Z., Riley, P., Lionello, R., and Odstrcil, D.: 2003, in M. Velli, R. Bruno, and F. Malara (eds.), *Proceedings of the 10th International Solar Wind Conference, AIP Conf. Proc.* **679**, Am. Inst. Phys., New York, p. 703.

Liu, Y., Richardson, J.D., and Belcher, J.W.: 2005, *Plan. Spa. Sci.* **53**, 3.

Luhmann, J.G., Li, Y., Arge, C.N., Gazis, P.R., and Ulrich, R.: 2002, *J. Geophys. Res*. **107**(A8), 1154, doi: 10.1029/2001JA007550.

Manchester, IV, W.B., Gombosi, T.I., Roussev, I., Ridley, A., De Zeeuw, D.L., Sokolov, I.V., Powell, K.G., and Tóth, G.: 2004, *J. Geophys. Res*. **109**, A02107, doi: 10.1029/2003JA010150.

Marsden, R.G., Sanderson, T.R., Tranquille, C., Wenzel, K.-P., and Smith, E.J.: 1987, *J. Geophys. Res*. **92**, 11009.

Marubashi, K: 1997, in N. Crooker, J.A. Joselyn, and J. Feynman (eds.), *Coronal Mass Ejections*, *Geophys. Monogr. Ser.*, AGU, Washington, DC, **99**, p. 147.

McComas, D.J., Bame, S.J., Barker, P., Feldman, W.C., Phillips, J.L., Riley, P., and Griffee, J.W.: 1998, *Spa. Sci. Rev.* **86**, 563.

Montgomery, M.D., Asbridge, J.R., Bame, S.J., and Feldman, W.C.: 1974, *J. Geophys. Res*. **79**, 3103.

Morrison, P.: 1956, *Phys. Rev.* **101**, 1397.

Neugebauer, M. and Goldstein, R.: 1997, in N. Crooker, J.A. Joselyn, and J. Feynman (eds.), *Coronal Mass Ejections*, *Geophys. Monogr. Ser.*, AGU, Washington, DC, **99**, p. 245.

Newbury, J.A., Russell, C.T., Phillips, J.L., and Gary, S.P.: 1998, *J. Geophys. Res*. **103**(A5), 9553.

Odstrcil, D. and Pizzo, V.J.: 1999a, *J. Geophys. Res*. **104**, 483.

Odstrcil, D. and Pizzo, V.J.: 1999b, *J. Geophys. Res*. **104**, 493.

Odstrcil, D. and Pizzo, V.J.: 1999c, *J. Geophys. Res*. **104**, 28225.

Ogilvie, K.W., Scudder, J.D., and Sugiura, M.: 1971, *J. Geophys. Res*. **76**, 8165.

Ogilvie, K.W., *et al.*: 1995, *Spa. Sci. Rev.* **71**, 55.

Osherovich, V. and Burlaga, L.F.: 1997, in N. Crooker, J.A. Joselyn, and J. Feynman (eds.), *Coronal Mass Ejections*, *Geophys. Monogr. Ser.*, AGU, Washington, DC, **99**, p. 157.

Palmer, I.D., Allum, F.R., and Singer, S.: 1978, *J. Geophys. Res*. **83**, 75.

Phillips, J.L., Bame, S.J., Feldman, W.C., Goldstein, B.E., Gosling, J.T., Hammond, C.M., McComas, D.J., Neugebauer, M., Scime, E.E., and Suess, S.T.: 1995, *Science* **268**, 1030.

Richardson, I.G. and Cane, H.V.: 1993, *J. Geophys. Res*. **98**, 15295.

Richardson, I.G. and Cane, H.V.: 1995, *J. Geophys. Res*. **100**, 23397.

Richardson, I.G. and Cane, H.V.: 2004, *Geophys. Res. Lett.* **31**, L18804, doi: 10.1029/2004GL020958.

Richardson, I.G. and Cane, H.V.: 2005, *AGU*, Abstr. Spring, SH43A-05

Richardson, I.G., Cane, H.V., and von Rosenvinge, T.T.: 1991, *J. Geophys. Res*. **96**, 7853.

Riley, P., Linker, J.A., Mikić, Z., Odstrcil, D., Zurbuchen, T.H., Lario, D., and Lepping, R.P.: 2003, *J. Geophys. Res*. **108**(A7), 1272.

Riley, P., Schatzman, C., Cane, H.V., Richardson, I.G., and Gopalswamy, N.: 2006, *Astrophys. J.* **647**, 648.

Russell, C.T. and McPherron, R.L.: 1973, *Spa. Sci. Rev.* **15**, 205.

Russell, C.T. and Shinde, A.A.: 2003, *Solar Phys*. **216**, 285.

Russell, C.T. and Shinde, A.A.: 2005, *Solar Phys*. **229**, 323.

Russell, C.T., Shinde, A.A., and Jian, L.: 2005, *Adv. Space Res.* **35**, 2178.

Rust, D.M.: 1999, *Geophys. Monogr.* **109**, 213.

Shodhan, S., Crooker, N.U., Kahler, S.W., Fitzenreiter, R.J., Larson, D.E., Lepping, R.P., Siscoe, G.L., and Gosling, J.T.: 2000, *J. Geophys. Res*. **105**(A12), 27261.

Smith, C.W., L'Heureux, J., Ness, N.F., Acuña, M.H., Burlaga, L.F., and Scheifele, J.: 1998, *Spa. Sci. Rev.* **86**, 613.

Spreiter, J.R., Summers, A.L., and Alksne, A.Y.: 1966, *Plan. Spa. Sci*. **14**, 223.

Steinberg, J.T., Gosling, J.T., Skoug, R.M., and Wiens, R.C.: 2005, *J. Geophys. Res*. **110**, A06103, doi: 10.1029/2005JA011027.

Zwickl, R.D., Asbridge, J.R., Bame, S.J., Feldman, W.C., Gosling, J.T., and Smith, E.J.: 1983, in M. Neugebauer (ed.), *Solar Wind Five*, NASA Conf. Publ. 2280, NASA, Washington, DC, p. 711.